



Source Apportionment of Carbonaceous Aerosols in Beijing with Radiocarbon and Organic Tracers: Insight into the Differences between Urban and Rural Sites

5 Siqi Hou^{1*}, Di Liu^{1,2}, Jingsha Xu¹, Tuan V. Vu^{1,3}, Xuefang Wu⁴, Deepchandra Srivastava¹, Pingqing Fu⁵, Linjie Li^{6,7}, Yele Sun⁶, Athanasia Vlachou⁸, Vaios Moschos⁸, Gary Salazar⁹, Sönke Szidat⁹, André S.H. Prévôt⁸, Roy M. Harrison¹, Zongbo Shi¹

¹ School of Geography Earth and Environmental Science, University of Birmingham, Birmingham, B15 2TT, UK

² Now at: Institute of Atmospheric Physics, Chinese Academy of Sciences, Beijing, 100029, China

³ Now at: School of Public Health, Imperial College London, London, UK

10 ⁴ School of Earth Sciences and Resources, China University of Geosciences, Xueyuan Road 29, 100083, Beijing, China

⁵ Institute of Surface-Earth System Science, Tianjin University, Tianjin 300072, China

⁶ State Key Laboratory of Atmospheric Boundary Layer Physics and Atmospheric Chemistry Institute of Atmospheric Physics, Chinese Academy of Sciences, Beijing, 100029, China

⁷ now at: Department of Chemistry and Molecular Biology, University of Gothenburg, Gothenburg 41296, Sweden

15 ⁸ Laboratory of Atmospheric Chemistry, Paul Scherrer Institute, Villigen PSI, CH-5232, Switzerland

⁹ Department of Chemistry and Biochemistry & Oeschger Centre for Climate Change Research, University of Bern, Bern, CH-3012, Switzerland

*Siqi Hou and Di Liu made equal contributions.

20 *Correspondence to:* Roy M. Harrison (r.m.harrison@bham.ac.uk), Zongbo Shi (z.shi@bham.ac.uk)

Abstract. Carbonaceous aerosol is the dominant component of fine particles in Beijing. However, it is challenging to apportion its sources. Here, we applied a newly developed method which combined radiocarbon (¹⁴C) with organic tracers to apportion the sources of fine carbonaceous particles at an urban (IAP) and a rural (PG) site of Beijing. PM_{2.5} filter samples (24-h) were collected at both sites from 10 November to 11 December 2016 and from 22 May to 24 June 2017. ¹⁴C was
25 determined in 25 aerosol samples (13 at IAP and 12 at PG) representing low pollution to haze conditions. Biomass burning tracers (levoglucosan, mannosan and galactosan) in the samples were also determined using GC-MS. Higher contributions of fossil-derived OC (OC_f) were found at the urban site. OC_f to OC ratio decreased in the summer samples (IAP: 67.8 ± 4.0% in winter and 54.2 ± 11.7% in summer; PG: 59.3 ± 5.7% in winter and 50.0 ± 9.0% in summer) due to less consumption of coal in the warm season. A novel extended Gelencsér method incorporating the ¹⁴C and organic tracer data was developed to
30 estimate the fossil and non-fossil sources of primary and secondary OC (POC and SOC). It showed that fossil-derived POC was the largest contributor to OC (35.8 ± 10.5% and 34.1 ± 8.7% in winter time for IAP and PG, 28.9 ± 7.4% and 28.9 ± 9.6% in summer), regardless of season. SOC contributed 50.0 ± 12.3% and 47.2 ± 15.5% at IAP, and 42.0 ± 11.7% and 43.0 ±



13.4% at PG in the winter and summer sampling periods respectively, within which the fossil-derived SOC was predominant and contributed more in winter. The non-fossil fractions of SOC increased in summer due to a larger biogenic component. Concentrations of biomass burning OC (OC_{bb}) are resolved by the extended Gelencsér method with average contributions (to total OC) of $10.6 \pm 1.7\%$ and $10.4 \pm 1.5\%$ in winter at IAP and PG, and $6.5 \pm 5.2\%$ and $17.9 \pm 3.5\%$ in summer, respectively. Correlations of water-insoluble OC (WINSOC), water-soluble OC (WSOC) with POC and SOC showed that although WINSOC was the major contributor to POC, a non-negligible fraction of WINSOC was found in SOC for both fossil and non-fossil sources especially during winter. In summer, a greater proportion of WSOC from non-fossil sources was found in SOC. Comparisons of the source apportionment results with those obtained from a Chemical Mass Balance model were generally good, except for the cooking aerosol.

1 Introduction

Carbonaceous aerosols, often one of the most abundant components (20-80%) in atmospheric aerosol particles, have a crucial impact on the global climate, air quality and human health (He et al., 2001; Huang et al., 2014; Jimenez et al., 2009; Song et al., 2007; Zhou et al., 2018). The total content of carbonaceous aerosols (i.e., total carbon, TC) can be divided into organic carbon (OC) and elemental carbon (EC) according to their physical, chemical and optical properties. The source of EC is from incomplete combustion of fossil fuel or biomass, while OC mainly originates from primary emissions from sources such as coal combustion, traffic emissions, cooking, and biomass burning as well as from gas-particle conversion (Yang et al., 2016). It is very challenging to quantify the contributions from different sources to OC and EC because of the limited information on the sources, atmospheric loading and composition of organic aerosols (Huang et al., 2014). Radiocarbon (^{14}C) analysis is a powerful tool for the quantification of fossil and non-fossil contributions to carbonaceous aerosols, as non-fossil sources contain a high contemporary ^{14}C content, while the fossil fractions are free of ^{14}C (Zotter et al., 2014; Bernardoni et al., 2013; Liu et al., 2013; Szidat et al., 2004; Szidat et al., 2006; Szidat et al., 2009). A previous study in north-east China found a dominant fossil-fuel contribution to EC ($76 \pm 11\%$), and that non-fossil sources are major contributors to OC ($66 \pm 11\%$) (Zhang et al., 2016). Non-fossil sources of OC were major contributors to the fine particle pollution in Beijing during the APEC summit (Liu et al., 2016a). Moreover, clear seasonal trends of non-fossil and fossil source contributions to water-insoluble OC (WINSOC) and water-soluble OC (WSOC) were found. Non-fossil sources were the major contributor (59%) to WINSOC in summer and autumn, whereas fossil fuel emissions were predominant in winter and spring (Liu et al., 2013). Proportions of non-fossil sources in TC and WSOC associated with biogenic emissions increased during spring and summer with maxima (85% and 117%, respectively) in May (Pavuluri et al., 2013). However, ^{14}C measurements do not permit direct discrimination of specific sources (e.g. biomass burning or secondary OC - SOC) of modern carbon. A combination with other techniques gives further insight into the characteristics of SOC (Minguillon et al.,



2011; Szidat et al., 2006; Szidat et al., 2009; Yttri et al., 2011). For example, applying Latin hypercube sampling with different OC/EC ratios, relative contributions of primary and secondary organic carbon were estimated (Zhang et al., 2016).
65 ¹⁴C analysis combined with AMS-PMF data has contributed to the identification of sources from primary emissions and secondary formation (Barrett et al., 2015; Zhang et al., 2018; Zhang et al., 2017; Vlachou et al., 2018).

The Gelencsér method provides a first-order source apportionment of organic aerosol from fossil fuel combustion, biomass burning, biogenic emissions and secondary organic aerosol, using measurements of specific organic tracers emitted by fossil and non-fossil sources and their OC/EC ratios derived from literature (Gelencsér et al., 2007). This method was derived in a
70 European context, but for China the inclusion of food cooking and coal combustion is required. Based upon this consideration, an extended Gelencsér method that includes quantification of fossil and contemporary EC and OC by ¹⁴C analysis has been developed in this study. The diversity of fuel types and combustion conditions make the selection of OC/EC ratios for biomass burning difficult due to large uncertainties. For non-fossil sources of SOC, quantification by the method of Gelencsér et al. (2007) is totally dependent on the source apportionment of OC from biomass burning, and thus a
75 cautious selection of ratios has been adopted in this study.

Biomass burning is an important source of both EC and OC, which can affect large areas of the world through long-range transport (Andreae and Merlet, 2001). It is also a key component when applying source apportionment by the Gelencsér method. As levoglucosan (1,6-anhydro-β-D-glucopyranose, LG) is an almost specific biomass burning tracer as the main pyrolysis product from cellulose (Puxbaum et al., 2007; Simoneit et al., 1999), concentrations of OC from biomass burning
80 can be obtained by multiplying LG with suitable OC/LG ratios (Gelencsér et al., 2007; Zdrahal et al., 2002). However, the wide range of OC/LG ratios associated with changes in the biofuel types and combustion conditions cause great uncertainty in the estimation (Cheng et al., 2013; Fu et al., 2012; Gelencsér et al., 2007). To mitigate these differences from types of material and the burning conditions, a typical ratio of 12.2–12.5 (12.3 on average) was documented in Andreae and Merlet (2001) by considering the biofuels of savanna and crop residues. This ratio is widely accepted in many studies (Andreae and
85 Merlet, 2001; Fu et al., 2012; Zhang et al., 2008a; Zhang et al., 2007), and has been used to estimate the contributions of biomass burning in Beijing which ranged from 8–50 % (Cheng et al., 2013; Kang et al., 2018; Liu et al., 2017; Zhang et al., 2008a; Zhang et al., 2017). However, a single ratio is not representative of all local conditions, and more specific methods are needed. ¹⁴C analysis can provide accurate concentrations of EC from biomass burning, assuming that EC from non-fossil sources is exclusively from biomass burning. Introducing EC_{nf} concentrations from ¹⁴C analysis into the Gelencsér method
90 of using OC/LG ratios provides valuable extra information, and allows the method to be extended to include other sources.

Beijing, capital of China, has experienced severe PM_{2.5} pollution for decades. This has been subjected to extensive research. However, few studies have sought to differentiate the fossil and non-fossil sources of SOC, even though they provide key



information on the precursors and formation mechanisms of SOC. In this study, measurements of PM_{2.5}, OC and EC along with biomass burning tracers were conducted simultaneously at urban and rural sites of Beijing in the winter of 2016 and summer of 2017. ¹⁴C measurements of EC, OC, WINSOC and WSOC were carried out subsequently on filter samples to enable source apportionment of fossil vs non-fossil sources. A novel extended Gelencsér method combining ¹⁴C analysis has been developed to explore the source apportionment of OC and EC, with SOC from fossil and non-fossil sources being quantified. The source apportionment results were compared with those by Chemical Mass Balance (CMB). Correlations of WINSOC and WSOC with different sources of OC were also performed to study the formation mechanisms of SOC.

100 2 Methodology

2.1 Aerosol Sampling

Daily PM_{2.5} (particles with aerodynamic diameter less than 2.5 μm) samples were collected at an urban site (39.98° N, 116.39° E, Institute of Atmospheric Physics, IAP), and a rural site (40.17° N, 117.05° E, Pinggu, PG) in Beijing during a winter campaign (10 November–11 December 2016) and a summer campaign (22 May–24 June 2017) as part of the Atmospheric Pollution and Human Health in a Chinese megacity (APHH-China) programme; further information on the sampling sites is available in Shi et al. (2019). The urban site is a typical urban background site but may be subject to multiple local influences such as cooking emissions from nearby restaurants. The rural site is located in Pinggu District, close to a village surrounded by farmland. It is ~60 km northeast from urban Beijing at the junction of Beijing, Tianjin and Hebei provinces. A two-lane road is about 200–300 meters north of the sampling site, but its traffic volume is relatively low.

110 Hi-Vol air samplers (Tisch, USA) with a flow rate of 1.1 m³ min⁻¹ were collected on pre-combusted (450 °C, 6 h) quartz filters (Pallflex, 8×10 inch). Field blanks were collected by placing filters onto the filter holder for a few minutes without pumping before and after the campaign. After sampling, each exposed or blank filter was wrapped individually with aluminium foil and stored at -20 °C in the dark prior to analysis. The details of the sample collection are described elsewhere (Shi et al., 2019).

115 2.2 Chemical Analysis

2.2.1 OC, EC and major inorganic ions

OC and EC mass concentrations were determined with the DRI2015 carbon analyser with the EUSAAR_2 (European Supersites for Atmospheric Aerosol Research) transmittance protocol. Replicate analyses were conducted once every ten samples. Blank samples (corresponding to 0.40 and 0.01 μg m⁻³ for OC and EC) were analysed to correct the sample results. The limits of detection of OC and EC were estimated to be 0.03 and 0.05 μg m⁻³. Details of the OC/EC measurement method



are described elsewhere (Paraskevopoulou et al., 2014). Major ions including SO_4^{2-} , NO_3^- , NH_4^+ , Na^+ , K^+ and Cl^- were determined on water extracts using an ion chromatograph (Dionex, Sunnyvale, CA, USA), with detection limits less than $0.01 \mu\text{g m}^{-3}$. The uncertainties for OC and EC were less than 10% and less than 5% for inorganic ions (Xu et al., 2020a).

2.2.2 Biomass Burning Tracers

125 The methodology to determine biomass burning tracers, including levoglucosan, mannosan and galactosan was described elsewhere (Fu et al., 2016). Recoveries for target compounds were better than 80 % as obtained by spiking standards to pre-combusted quartz filters followed by extraction and derivatization. Field blank filters were analysed by the procedure used for the samples above, but no target compounds were detected. Duplicate analyses showed analytical errors less than 15 %.

2.3 Radiocarbon (^{14}C) Analysis

130 The ^{14}C in total carbon (TC), water-insoluble TC (WINSTC) and EC was determined on 25 (13 from IAP and 12 from PG) time-integrated Hi-Vol $\text{PM}_{2.5}$ quartz fibre (QF) filter samples. Samples collected during both haze and non-haze days were selected in winter to better understand the pollution sources. $\text{PM}_{2.5}$ concentrations on 22 November and 1 December at IAP and PG sites were lower than $75 \mu\text{g m}^{-3}$ and regarded as non-haze air days, in contrast to other wintertime samples collected during haze pollution days. During the summer, typical samples were selected with $\text{PM}_{2.5}$ concentrations of 42.5 ± 26.5 and
135 $42.7 \pm 21.2 \mu\text{g m}^{-3}$ at IAP and PG, respectively. The concentrations of $\text{PM}_{2.5}$, EC, OC and the corresponding non-fossil fractions of these selected days are shown in Table S1.

The method of ^{14}C measurement of carbonaceous aerosols has been described elsewhere (Agrios et al., 2015; Levin et al., 2010; Szidat et al., 2014; Vlachou et al., 2018; Zhang et al., 2012; Zhang et al., 2016; Zotter et al., 2014). The ^{14}C of TC and WINSTC was measured by using an one-step protocol under pure O_2 (99.9995%) at $760 \text{ }^\circ\text{C}$ for 400 s (Vlachou et al., 2018)
140 using an Elemental Analyzer coupled with the accelerator mass spectrometer Mini Carbon Dating System (MICADAS) at the Laboratory for the Analysis of Radiocarbon (LARA, University of Bern) (Zhang et al., 2012; Szidat et al., 2014). The EC fraction was separated by an OC/EC analyser (Model 4L, Sunset Laboratory, USA) with the use of the Swiss_4S protocol (Zhang et al., 2012), which was coupled online with the MICADAS (Agrios et al., 2015). Each filter sample was extracted with water before the measurements to minimize the charring effect during the separation of EC from the WINSOC.

145 ^{14}C results were expressed as fractions of modern (f_M), i.e., the fraction of the $^{14}\text{C}/^{12}\text{C}$ ratio of the sample related to that of the reference year 1950. The data analysis was carried out accounting for the blank correction (one field blank per site was analysed, not relevant for EC), decay of ^{14}C since the 1950's, nuclear bomb correction, charring of WINSOC (~1%) and EC yield after OC removal (IAP: $62 \pm 6\%$; PG: $76 \pm 8\%$) (Zhang et al., 2012; Zhang et al., 2016; Zotter et al., 2014).



Non-fossil fractions (f_{NF}) were determined from their corresponding f_M values and reference values for pure non-fossil
150 sources by:

$$f_{NF} = \frac{f_M}{f_{NF,ref}} \quad (1)$$

Different values for the $f_{NF,ref}$ were applied for the bomb peak correction (Levin, et al. 2010). For EC, the f_M is 1.10 ± 0.05
(Lewis et al., 2004; Palstra and Meijer, 2014), given that biomass burning is assumed to be the only non-fossil source of EC.
For OC, it is calculated as

155 $f_{NF,ref} = p_{bio} \times f_{M,bio} + p_{bb} \times f_{M,bb}$ (2)

where $f_{M,bb}$ and $f_{M,bio}$ is coming from biomass burning and biogenic sources respectively, which are 1.10 ± 0.05 and $1.023 \pm$
 0.015 (Lewis et al., 2004; Zotter et al., 2014), while p_{bio} and p_{bb} are the proportions of biogenic source and biomass burning
respectively, which are 0.9 and 0.1 in winter and 0.5 and 0.5 in summer (Levin et al., 2010).

Analogously, the non-fossil fractions of OC, WSOC and WINSOC ($f_{NF,OC}$, $f_{NF,WSOC}$ and $f_{NF,WINSOC}$) were calculated by
160 following a mass balance-like approach:

$$OC_{nf} = OC \times f_{NF,OC} = TC \times f_{NF,TC} - EC \times f_{NF,EC} \quad (3)$$

$$WSOC_{nf} = WSOC \times f_{NF,WSOC} \approx WSOC \times f_{NF,WSTC} = TC \times f_{NF,TC} - WINSTC \times f_{NF,WINSTC} \quad (4)$$

$$WINSOC_{nf} = WINSOC \times f_{NF,WINSOC} = OC \times f_{NF,OC} - WSOC \times f_{NF,WSOC} \quad (5)$$

where TC and EC are the concentrations of total and elemental carbon, respectively, and $f_{NF,TC}$, $f_{NF,EC}$, $f_{NF,WINSTC}$ are the non-
165 fossil fractions of TC, EC and WINSTC, respectively. The fraction of fossil-fuel sources was calculated by $f_{FF} = 1 - f_{NF}$. The
uncertainties were determined by error propagation. The mass concentration errors were assumed to be 10 % for EC and 6 %
for OC and TC (typical values for EUSAAR2) (Zhang et al., 2016).

2.4 Extended Gelencsér method including ^{14}C data

An extended Gelencsér method including ^{14}C data was developed to quantify the fossil and non-fossil sources of primary and
170 secondary OC (POC and SOC) along with OC from biomass burning and cooking (OC_{bb} and OC_{ck}). The equations for the
extended Gelencsér method are list in Table 1. The detailed selection of the OC/EC ratios will be discussed in Sect. 3.2.



2.5 Chemical Mass Balance (CMB) model and AMS/ACSM-PMF Analysis

Results on the same sets of samples from a chemical mass balance (US EPA CMB8.2) model and AMS/ACSM-PMF analysis (Positive matrix factorization analysis of data from online Aerodyne Aerosol Mass Spectrometer at IAP and Aerosol
175 Chemical Speciation Monitor at PG) were compared with ^{14}C -based source apportionment. Details on the experimental details and data analyses can be found in Xu et al. (2020b) and Wu et al. (2020). The CMB utilizes a linear least squares solution considering both uncertainties in source profiles and ambient measurements to ensure reliable fitting results. In order to better represent the source characteristics, the source profiles applied in this model were mostly from local studies in China (Cai et al., 2017; Wang et al., 2009; Zhang et al., 2007; Zhang et al., 2008b; Zhao et al., 2015), except vegetative
180 detritus (Rogge et al., 1993; Wang et al., 2009). The detail of selecting organic marker species can be found in Yin et al. (2010; 2015).

Experimental details of the AMS and ACSM-PMF method can be found elsewhere (Ng et al., 2011; Sun et al., 2016; Xu et al., 2019). The ACSM data were analysed for the mass concentrations and size distributions of non-refractory submicron aerosol (NR- PM_{10}) species using the high-resolution data analysis software package PIKA (Sun et al., 2020). Positive matrix
185 factorization was performed on high-resolution mass spectra of V-mode and W-mode to retrieve potential OA factors from different sources (Paatero and Tapper, 1994; Ulbrich et al., 2009). The OM/OC factor used for cooking OA (COA) is 1.38 (Xu et al., 2019).

3 Results and discussion

3.1 Overall results

190 3.1.1 Characteristics of $\text{PM}_{2.5}$, OC and EC concentrations

Mass concentrations of $\text{PM}_{2.5}$, OC, EC and biomass burning tracers are shown in Fig. 1 and are summarized in Table 2 along with the meteorological conditions during the observation campaign in IAP and PG. The average concentrations of $\text{PM}_{2.5}$ were $91.2 \pm 63.7 \mu\text{g m}^{-3}$ and $99.7 \pm 77.8 \mu\text{g m}^{-3}$ at the IAP and PG sites respectively in winter, and $30.2 \pm 14.8 \mu\text{g m}^{-3}$, and $27.5 \pm 12.9 \mu\text{g m}^{-3}$ at the IAP and PG sites in summer. The highest 24-h concentration in winter is $239.9 \mu\text{g m}^{-3}$ (IAP) and
195 $294.3 \mu\text{g m}^{-3}$ (PG), and more than 53 % and 46 % of the days have a daily $\text{PM}_{2.5}$ concentrations higher than the Chinese air quality standard ($\text{PM}_{2.5}$ concentrations exceeding $75 \mu\text{g m}^{-3}$ are defined as haze conditions) in IAP and PG during the observation period. In summer, the air quality was improved, with $\text{PM}_{2.5}$ concentrations ranging from 12.2 to $78.8 \mu\text{g m}^{-3}$ and 11.6 to $70.3 \mu\text{g m}^{-3}$ in IAP and PG, respectively.

Organic carbon and elemental carbon (OC and EC) are important constituents of $\text{PM}_{2.5}$, accounting for $30.9 \pm 9.3 \%$ and 43.6
200 $\pm 17.9 \%$ of $\text{PM}_{2.5}$ mass at the IAP and PG sites in winter, and $26.8 \pm 9.2 \%$ and $37.3 \pm 12.6 \%$ in summer. The



concentrations of EC showed a strong correlation with OC at both sites during the winter and summer (Table 3). The average EC concentrations for ^{14}C analysis varied from $3.8 \pm 2.1 \mu\text{g m}^{-3}$ (IAP) and $5.4 \pm 2.6 \mu\text{g m}^{-3}$ (PG) in winter and $1.1 \pm 0.3 \mu\text{g m}^{-3}$ (IAP) and $2.0 \pm 0.7 \mu\text{g m}^{-3}$ (PG) in summer for the urban and rural sites respectively. The mass concentration of OC for ^{14}C analysis was $4.1\text{--}44.9 \mu\text{g m}^{-3}$ and $12.1\text{--}85.0 \mu\text{g m}^{-3}$ at IAP and PG in winter, and $4.7\text{--}12.7 \mu\text{g m}^{-3}$ and $6.2\text{--}17.9 \mu\text{g m}^{-3}$ in
205 summer. The selected samples are well representatives as their concentrations were very close to those from the whole campaign. The average OC concentration for ^{14}C in winter was 3.2 and 4.3 times higher than in summer at IAP and PG, respectively. The OC/EC ratios at IAP and PG were in the range of 4.1–14.9 and 6.2–14.6 in winter, and 4.6–14.8 and 4.4–28.3 in summer, which were all higher than 2.0 or 1.1 (Chow et al., 1996; Castro et al., 1999), suggesting an important contribution from secondary organic carbon (SOC).

210 3.1.2 Fossil and non-fossil sources of EC and OC based on radiocarbon (^{14}C) analysis

Fig. 2 shows the absolute concentrations of fossil and non-fossil fractions of OC and EC, and the relative contributions. EC_f refers to EC from coal combustion and liquid fossil fuel (i.e., mainly vehicle emissions) and EC_{nf} from biomass burning (Gray and Cass 1998). As shown in Fig. 2, high concentrations of EC_f and EC_{nf} were found in both urban and rural sites in winter, suggesting elevated emissions from primary fossil and non-fossil sources like coal combustion and biomass burning.
215 Residential coal consumption and biomass burning are still important in winter especially in rural areas, due to intensive heating activities in the cold season. EC_f contributed $7.6 \pm 2.1 \%$ and $6.0 \pm 1.4 \%$ to TC at the IAP and PG sites in winter and $6.9 \pm 1.6 \%$ and $8.9 \pm 2.6 \%$ in summer. Most of the fossil fractions of EC are within the range of previous studies in urban Beijing (67–96% of EC) (Liu et al., 2020; Liu et al., 2017; Zhang et al., 2016; Zhang et al., 2017). Higher contributions of EC_f were found on the polluted days in wintertime (Table S1), showing that the $\text{PM}_{2.5}$ concentrations may be elevated due to
220 direct emission from coal combustion and vehicle exhaust. Fractions of EC_{nf} increased slightly in summer due to the regional open burning activities during the post-harvest period of wheat, which is common in Northern China (Li et al., 2016; Yan et al., 2006).

OC from fossil sources (OC_f) arises mainly from coal combustion and vehicle emissions, while OC from non-fossil sources (OC_{nf}) comes mainly from biomass burning, biogenic emissions and cooking. Although fossil sources are the main contributor to OC ($67.8 \pm 4.0 \%$ and $59.3 \pm 5.7 \%$ at IAP and PG sites in winter, compared to $54.2 \pm 11.7 \%$ and $50.0 \pm 9.0 \%$ in summer), relative contributions of OC_{nf} were significantly increased in summer. These results are similar to a previous study in urban Beijing, which found a contribution of $66 \pm 11 \%$ ranging from 45 to 82 % in PM_1 collected in 2013–2014 (Zhang et al., 2017). The increased contribution of OC_{nf} in summer is likely to due to the enhancement of biomass burning and biogenic emissions (both primary and through SOC) as well as the decline in emissions from fossil sources such as coal
225 burning, considering that cooking OC emission is unlikely to change with season.
230



Fossil and non-fossil sources of WSOC and WINSOC were also quantified by the ^{14}C measurement. Among the four fractions, WINSOC_f had the highest contribution to TC in winter (37.9 ± 4.5 % at IAP and 36.2 ± 4.7 % at PG) followed by WSOC_f (22.1 ± 5.2 %) at IAP and WINSOC_{nf} (20.8 ± 3.4 %) at PG. In summer, the fraction of WINSOC_f fell to 24.4 ± 9.3 % at IAP and 21.8 ± 4.6 % at PG, accompanied by increased fossil and non-fossil contributions from WSOC fractions. The increase of WSOC_f fractions in summer implied an enhanced contribution from oxidised VOCs and aged primary fossil-derived OC, and WSOC_{nf} is probably associated with biomass burning and secondary OC. Moreover, WINSOC was dominated by fossil sources at both sites in winter (IAP: 72.6 ± 3.6 %; PG: 63.4 ± 6.5 %), while the non-fossil fractions significantly increased from winter to summer. Similarly, WSOC was mainly fossil-derived in winter, while it tends to be accumulated in non-fossil fractions in summer (fossil fraction in WSOC, IAP: 60.5 ± 6.6 % in winter, 50.8 ± 12.3 % in summer; PG: 51.6 ± 8.7 % in winter, 47.7 ± 17.4 % in summer). The contribution of OC_{nf} to OC increased with both non-fossil fractions in WINSOC and WSOC increasing. Even though WINSOC_{nf} and WSOC_{nf} cannot be attributed specifically to biomass burning, biogenic emissions, cooking or secondary formation, it is likely that biogenic-derived POC and SOC make a pronounced contribution. Details of contributions of each fraction to primary and secondary OC will be discussed in Sect. 3.2.

3.2 Source apportionment by an extended Gelencsér method

Gelencsér et al. (2007) reported a method for the source apportionment of carbonaceous aerosol into fractions from biomass burning, road traffic and secondary organic aerosol, applicable to Europe where these are the dominant sources. In order to use the same methodological concepts in China, the method required extending to include two further sources: coal combustion and cooking. To do so, the ^{14}C data were utilized.

3.2.1 Biomass burning

Levoglucosan (LG) is a typical biomass burning tracer, as the main pyrolysis product from cellulose. Much higher concentrations of LG were observed in the winter (311 ± 193 ng m⁻³ at IAP and 634 ± 483 ng m⁻³ at PG) than those in the summer (27.9 ± 29.6 ng m⁻³ at IAP and 74.0 ± 34.2 ng m⁻³ at PG). In addition, LG concentrations at the rural site were higher than those at the urban site in both winter and summer. This pattern is consistent with previous measurements in Table 4 (Chen et al., 2018; Kang et al., 2018; Li et al., 2018; Liu et al., 2016b; Salma et al., 2017; Sullivan et al., 2019; Yan et al., 2019; Zhu et al., 2017). The Pearson correlations of LG with PM_{2.5}, OC and EC at IAP and PG are shown in Table 3. During winter, LG correlated well with PM_{2.5}, OC and EC at PG with correlation coefficients of 0.89, 0.89 and 0.81 respectively. These are higher than those at IAP (correlation coefficients of 0.56, 0.60 and 0.74, respectively), suggesting a more significant influence of biomass burning upon PM_{2.5} in PG. The correlation coefficients in summer were much lower than those in winter for both sites, evidencing a reduced contribution of biomass burning activities to PM_{2.5}. During the



wintertime, the increasing use of biofuel for heating exacerbates the biomass pollution, and the stable atmospheric conditions also enhance the accumulation of LG (Shi et al., 2019). Compared with widely used cleaner fossil energy (i.e., natural gas, electricity, and liquefied petroleum gas) and renewable energy (i.e., solar energy) available in urban areas, the rural households are still largely using straw and wood for cooking and heating (Hou et al., 2017). Moreover, open burning of crop residues during the post-harvest months (May to July and October to November in North China) in rural areas is still frequently performed in spite of prohibition by the government (Chen et al., 2017; Li et al., 2016). Water-soluble potassium ion (K^+) has been used as biomass burning tracer previously, due to its good relationship with LG. However, in this study, the Pearson correlation coefficients of K^+ with LG are 0.51 and 0.86 in winter and 0.85 and 0.51 in summer for IAP and PG (Table 3), indicating other non-biomass sources of K^+ . Indeed, the sources of K^+ in the atmosphere are diverse, including sea salt, cooking, dust, coal combustion, and waste incineration, which makes K^+ less suitable as biomass burning tracer (Zhang, et al., 2010).

According to Gelencsér et al. (2007), EC from biomass burning (EC_{bb}) can be derived by multiplying the LG concentrations first with $(OC/LG)_{bb}$ to give OC_{bb} and then with $(EC/OC)_{bb}$. However, the $(OC/LG)_{bb}$ ratio is highly variable depending on the type of material and the conditions of burning, and the ratios can vary by orders of magnitude. Therefore, EC concentrations from non-fossil sources determined by radiocarbon analysis (EC_{nf}), assumed to arise almost solely from biomass burning were used as an estimate of EC_{bb} . Hence,

$$EC_{nf} \approx EC_{bb} = LG \times (OC/LG)_{bb} \times (EC/OC)_{bb} \quad (6)$$

The ratios of levoglucosan to mannosan (LG/MN) and to galactosan (LG/GA) can help us to infer the $(OC/LG)_{bb}$ and $(EC/OC)_{bb}$ ratios from certain types of biomass fuel (Kawamura et al., 2012). Fig. 3 shows the source profile for LG/MN and LG/GA ratios measured in emissions from controlled biomass burning experiments in previous studies (Cheng et al., 2013; Sun et al., 2019a; 2019b). There is a clear boundary of LG/MN ratios (~ 10) between softwood and hardwood burning (Kawamura et al., 2012). Using LG/GA ratios can help to identify the burning of straws, woods, needles and grasses, where most of the LG/GA ratios from burning of hardwood, straws and grasses are higher than 10, apparently different from those of needle plants. LG/MA and LG/GA ratios cannot be used to separate the burning of straws from hardwood, but the burning of hardwood can be neglected considering the local forest types around Beijing (Cheng et al., 2013).

The measured LG/MN and LG/GA ratios in this study (Fig. 3) implied that the use of biofuels was mainly a mixture of softwood and crop straws. Compared with ratios in summer, LG/MN and LG/GA ratios in winter have a narrower range at both IAP and PG sites and most of them converge at values lower than 10, suggesting wood burning may be dominant in winter and the contribution of straw burning increases in summer. It has been reported that firewood burning emissions in



290 Beijing represent 47–90 % of the total biomass burning, and could contribute more than 80 % in winter (Zhou et al., 2017). Although the LG/MN and LG/GA ratios of maize burning and wheat burning are similar and cannot be used to distinguish the two, research into the yield of main crops and farming practices showed that the main straw burning in Beijing and nearby provinces may be associated with maize straw in October to November and wheat straw in May to July (Zhang et al., 2019).

295 These results suggest that softwood burning and straw burning are the main sources of aerosols from biomass burning in Beijing. Thus, EC from softwood burning and straw burning can be calculated as follows:

$$\begin{aligned} EC_{nf} &\approx EC_{bb} = EC_{wood} + EC_{straw} \\ &= LG \times f_{wood} \times (OC/LG)_{wood} \times (EC/OC)_{wood} + LG \times f_{straw} \times (OC/LG)_{straw} \times (EC/OC)_{straw} \end{aligned} \quad (7)$$

where, f_{wood} represents the fraction of LG from softwood burning, and f_{straw} represents the fraction of LG from straw burning.
 300 $f_{straw} = 1 - f_{wood}$, neglecting other sources of biomass burning. f_{wood} can be expressed as,

$$f_{wood} = \frac{EC_{nf} - LG \times (OC/LG)_{straw} \times (EC/OC)_{straw}}{((OC/LG)_{wood} \times (EC/OC)_{wood} - (OC/LG)_{straw} \times (EC/OC)_{straw}) \times LG} \quad (8)$$

As f_{wood} should in the range of 0~1, it can be used as the limits of selected EC/OC and OC/LG ratios from softwood and straw. The details of the ratio selection can be found in the Supplement. Once values of f_{wood} are confirmed, OC from softwood (OC_{wood}) and straw burning (OC_{straw}) can be obtained by:

$$305 \quad OC_{wood} = LG \times f_{wood} \times (OC/LG)_{wood} \quad (9)$$

$$OC_{straw} = LG \times (1 - f_{wood}) \times (OC/LG)_{straw} \quad (10)$$

$$OC_{bb} = OC_{wood} + OC_{straw} \quad (11)$$

The mass concentrations of OC_{bb} and the contributions of OC_{wood} and OC_{straw} are shown in Fig. 4. The average concentration of OC_{bb} in IAP winter was $2.7 \pm 1.3 \mu\text{g m}^{-3}$, with a contribution of $10.6 \pm 1.7 \%$ to total OC, which is about half that in PG winter ($4.8 \pm 2.4 \mu\text{g m}^{-3}$, $10.4 \pm 1.5 \%$). The OC_{bb} concentrations fell in summer ($0.6 \pm 0.7 \mu\text{g m}^{-3}$ at IAP, $2.0 \pm 0.8 \mu\text{g m}^{-3}$ at PG), the contributions are $6.5 \pm 5.2 \%$ and $17.9 \pm 3.5 \%$, respectively. The rural site always has a higher OC_{bb} , which is consistent with our previous discussions. OC_{wood} normally dominated OC_{bb} while the increase of OC_{straw} fraction may be attributed to the local open burning activities. The contributions of OC_{bb} in this study are slightly different from previous studies (Table 4), with lower percentage contributions in the winter sampling period. However, if applying a value of 12.2, a



315 typical OC/LG ratio widely used in previous studies (Andreae and Merlet, 2001; Fu et al., 2012; Zhang et al., 2008a; Zhang et al., 2007), contributions of OC_{bb} to OC would be 17.7 % and 26.3 % for IAP and PG in winter, 6.1 % and 10.8 % in summer, respectively. Compared with the results in this study, the ratio 12.2 may significantly overestimate the contributions of biomass burning in winter and underestimate the contributions in summer.

In addition, coal combustion may also emit LG, accounting for about 7 % of LG in Beijing (Yan et al., 2018; Zhang et al., 2008b). Considering that the reported LG/MN and LG/GA ratios of coal combustion (both are in the range of 5–10) are close to those in our measurements, there may be a contribution from coal burning to levoglucosan, but if this amounts to 7 % of levoglucosan, the percentage contribution of biomass burning to OC in winter falls to 10.3 ± 1.6 % and 10.2 ± 1.5 % at IAP and PG respectively.

Besides the local emissions, regional transport of air masses can elevate the local OC and EC concentrations. To study the influence of regional transport on biomass burning particles, back trajectories and fire spots are plotted in Fig. S1 and Fig. S2. As shown in Fig. S1, air masses at IAP and PG in winter originated in from Hebei, Shanxi and Inner Mongolia, and the fire spots showed low intensity of open burning activities along the air mass transport path during the measurement period. It suggests a less important effect of open burning through regional transport. During the summer, the open burning activities were greatly increased due to the harvesting of wheat (Zhang et al., 2019), which is confirmed by the fire spots distribution in Fig. S2. Air masses from Hebei, Liaoning and Shandong provinces, which contain particles from wheat straw burning, may have enhanced the concentrations of OC and EC in Beijing. Considering the open burning of straw is linked with a sudden increase of LG in the ambient atmosphere, the high LG concentrations accompanied with low fire spot intensity suggests a strong local emission, while days with high fire spot intensities may also be affected by regional transport. Combining the analysis of fire spots intensity and the OC_{wood} fractions can help to identify the influence of local emissions and regional transport. The details of regional transport and sources of biomass burning are summarized in Table S2.

3.2.2 Other sources of OC and consistency with CMB and ASCM-PMF model results

More detailed source apportionment of OC can be achieved by combining ^{14}C analysis with primary OC/EC ratios for each source. POC_f can be determined from EC_f with primary fossil-fuel OC/EC emission ratios $(POC/EC)_f$. However, the $(POC/EC)_f$ ratios in previous studies (1.12–2.08 in winter, 0.40–0.77 in summer, Zhang et al., 2017) give much lower POC_f values compared to CMB results (Fig. S5) even though mostly good correlations were found. In reality, $(POC/EC)_f$ ratios vary greatly according to combustion conditions, fuel types and even measurement method for OC and EC (Chow et al., 2001; Han et al., 2016), and it is very hard to accurately predict the $(POC/EC)_f$ ratio for a given area. Hence, we used the lowest $(OC/EC)_f$ ratios $(OC/EC)_{f, \min}$ as the $(POC/EC)_f$ to estimate POC_f . Due to the limited number of samples for ^{14}C analysis, the measured lowest $(OC/EC)_f$ ratios may be higher than the ratios for the whole sampling period, which will result



345 in an overestimation of POC_f . It is necessary to evaluate $(\text{OC}/\text{EC})_{f, \min}$ ratios for the whole sampling period. The evaluation method is described in the Supporting Information. In the same way, primary OC from non-fossil sources (POC_{nf}) can be calculated from EC_{nf} and lowest $(\text{OC}/\text{EC})_{\text{nf}}$ ratios, thereby concentrations of secondary OC from fossil sources (SOC_f), non-fossil sources (SOC_{nf}) and OC from cooking (OC_{ck}) can be obtained by equations in Table 1. The averaged source apportionment results are presented in Table 5.

350 Primary fossil-derived OC is mainly from coal combustion and traffic emissions in China. However, it cannot be distinguished by ^{14}C analysis. OC/EC ratios from coal combustion and traffic emissions are dependent on various factors, such as the types of coal, stoves, engines, the vehicle operating modes and test method. Typical OC/EC ratios of coal combustion and traffic emissions in Beijing are 2.38 ± 0.44 and 0.85 ± 0.16 , respectively (Ni et al., 2018). An upper limit of POC from traffic emissions (POC_{tr}) can be obtained by multiplying EC_f with the $(\text{OC}/\text{EC})_{\text{tr}}$ ratio (0.85 ± 0.16) considering
355 all EC_f to come from traffic emissions. A lower limit of POC from coal combustion (POC_{cc}) is obtained by subtracting POC_{tr} from POC_f . Such calculation shows that POC_{cc} dominated POC at both sites in winter and summer campaigns. The maximum contribution of POC_{tr} to OC was 7.3 % and 5.7 % in winter, and 6.8 % and 8.9 % in summer, for IAP and PG respectively, and POC_{cc} contributed at least 28.5 % and 28.4 % to OC for IAP and PG in winter, and 22.2 % and 20.0 % in summer.

360 This is a relatively crude method for source apportionment of primary OC from fossil and non-fossil sources. Therefore, further comparisons with results from application of a CMB method and from application of PMF to ACSM data were conducted to understand the uncertainties in source apportionment from different methods. The source contributions to OC at the IAP and PG sites in winter and summer from the CMB model (Xu et al., 2020b; Wu et al., 2020) are presented in Table 5. In brief, seven primary OC sources were apportioned, including emissions from vegetative detritus, biomass
365 burning, cooking, gasoline vehicles, diesel engines, industrial coal combustion, residential coal combustion, along with Other (secondary) OC. Among these sources, coal combustion (the total of residential and industrial coal combustion) accounted for 32.6 % to OC at IAP in winter and 40.0 % to OC at PG in summer, while other OC dominated OC at IAP in summer and at PG in winter, with contributions of 48.2 % and 32.5 %, respectively.

For comparison, OC from gasoline vehicles, diesel engines, industrial coal combustion and residential coal combustion
370 resolved by the CMB model are summed up as POC_f , and OC from vegetative detritus, biomass burning and cooking are summed up as POC_{nf} . Correlations of different OC sources from the extended Gelencsér method (EG method) and from the CMB model are shown in Fig. 5. Good correlations were found for POC_f , POC_{nf} , SOC and OC_{bb} despite the combination of sites and seasons ($R^2=0.96, 0.74, 0.85$ and 0.91). The EG method reported lower POC_f , POC_{nf} , and OC_{bb} values than those from CMB with slopes of 0.77, 0.66 and 0.53, respectively. More specifically, OC_{bb} by the EG method is 51 % of that by



375 CMB in winter, but 1.33 times higher than CMB in summer (Fig. S6). The main discrepancy within the apportionment of
OC_{bb} is caused by different parameters for the calculations. As the CMB model used source profiles from three major types
of cereal straw (wheat, corn, and rice) and two types of wood (pine and mixed wood), it may lead to an overestimation of OC
from straw burning. Closer values of POC_{nf} and SOC were found between the two methods in summer, when samples are
almost all belonging to the non-haze period (Fig. S6, Fig. S7). It indicated that the EG method may perform better when OC
380 concentrations are low. Although poor agreement of OC_{ck} was found between the EG method and the CMB model, the
former correlated better with results from the application of PMF to AMS/ACSM data (slope=0.74, R²=0.61). It had
previously been shown that discrepancies existed between CMB and PMF model in the quantification of OC_{ck}. ACSM-PMF
may overestimate OC_{ck} by approximately 2 times (Reyes-Villegas, et al., 2018; Yin et al., 2015), whereas, CMB may not be
sensitive enough to the source profile of cooking aerosols (Abdullahi et al., 2018). Overall, the EG method resolves primary
385 and secondary sources of OC well.

Fractions of POC_f, SOC_f, OC_{bb}, OC_{ck} and SOC_{nf} in OC are shown in Fig. 6. POC_f was the largest contributor to OC at both
sites through winter and summer. Comparable contributions of POC_f were observed at the urban and rural sites, which
reached to 35.8 ± 10.5 % and 34.1 ± 8.7 % in wintertime, and fell to 28.9 ± 7.4 % and 29.1 ± 9.4 % in summer, respectively.
Pronounced POC_f in wintertime especially during haze period implied a significant elevation of coal combustion and traffic
390 emissions. Fossil and non-fossil sources of SOC are distinguished by the EG method in this study for the first time. Average
contributions to OC from SOC_f are higher in winter. They decreased from 32.0 ± 12.5 % to 25.2 ± 7.6 % at IAP, and from
25.2 ± 10.4 % to 21.0 ± 14.4 % at PG from winter to summer. The contributions of SOC_{nf} are slightly greater in summer
(18.0 ± 2.9 %, 22.0 ± 17.6 % for IAP in winter and summer and 16.9 ± 10.8 %, 21.9 ± 16.4 % for PG in winter and summer,
respectively). Significant contributions of SOC_f in the winter sampling period indicated a greater fraction of OC_f from ageing
395 and oxidation. The elevated contributions of SOC_{nf} (as a percentage) in the summer sampling period may be assigned to the
reduced coal combustion and enhanced biogenic-derived SOC formation. Similar variations of SOC_f and OC_{onf} (all OC from
non-fossil sources excluding OC_{bb}) between winter and summer were found in the urban area of Beijing by Zhang et al.
(2016). The total SOC accounts for 50.0 ± 12.3 % and 42.0 ± 11.7 % of OC for IAP and PG site in winter, demonstrating an
important role of secondary formation processes especially at the urban site. The average contributions of OC_{ck} were 3.6 ±
400 2.7 % and 13.4 ± 5.8 % in winter for IAP and PG, and 17.4 ± 12.5 % and 10.4 ± 6.7 % in summer, close to those estimated
in previous studies (19 ± 4 %, Zhang et al., 2017). The slightly lower value of the OC_{ck} contribution in winter at the IAP site
(Fig. 5) was due to OC_{bb} being the overwhelming contributor to POC_{nf}.



3.2.3 Correlations of WINSOC, WSOC with POC and SOC

In order to better understand the origins and formation mechanism of OC, the correlations among WINSOC, WSOC, POC, SOC, OC_{bb} and OC_{ck} were investigated (Fig. 7). The regression slopes and correlation coefficients among them are summarized in Table S5. WINSOC_f is usually seen as a proxy of primary fossil-derived OC in many previous studies (Liu et al., 2016; Miyazaki et al., 2006), and in our study WINSOC_f correlated well with calculated POC_f by the EG method (R^2 of 0.97, 0.93, 0.97 and 0.82 for IAP and PG in winter and summer, respectively); good correlations were also observed between WINSOC_f and SOC_f with slopes of 1.54, 1.27, 0.99 and 0.99 for IAP and PG in winter and summer (corresponding R^2 is 0.96, 0.89, 0.91 and 0.43). The high WINSOC_f to SOC_f ratios implied a non-negligible fraction of WINSOC_f in SOC_f. Moreover, the ratios of WINSOC_f to POC_f decreased from winter to summer compared to the WSOC_f to POC_f ratios increasing, indicating a non-negligible fraction of WSOC_f in POC_f in summer. WSOC_{nf} and WINSOC_{nf} show good correlations with SOC_{nf} with larger WINSOC_{nf} to SOC_{nf} ratios in winter. The lower water solubility of SOC_f and SOC_{nf} in winter may be due to them originating from the less oxidized semi-volatile POC from wood burning and anthropogenic emission at low temperatures (Favez et al., 2008; Sciare et al., 2011). Weak photochemical activity would also lead to the formation of less oxidized SOC which is more water-insoluble (Donahue et al., 2006; Robinson et al., 2007). Significant contributions of WINSOC to SOC have been reported in France (Sciare et al., 2011) and Switzerland (Zhang et al., 2016). OC_{bb} correlated well with WSOC_{nf} (R^2 of 0.94, 0.92, 0.93 and 0.93, at IAP and PG in winter and summer) as it is mainly composed of polar and highly oxygenated compounds (Miyazaki et al., 2006). However, more pronounced WINSOC_{nf} in OC_{bb} was found in winter especially at the rural site. It seems that more water-insoluble fractions were observed in primary OC (POC_f, POC_{nf}, OC_{bb} and OC_{ck}) at the rural site in both winter and summer. It implies the emitted primary OC at the rural site was probably fresher, and hence less aged and oxidized. On the other hand, the source emission profile at rural sites may be different from urban sites, with more heavy-duty diesel trucks with a high content of water-insoluble OC emitted in rural areas.

4 CONCLUSIONS

Measurements of PM_{2.5}, OC, EC and biomass burning tracers were conducted at both urban and rural sites of Beijing from 10 November to 11 December 2016 and from 22 May to 24 June 2017, accompanied by the ¹⁴C analysis of 25 selected samples. On most days, fossil sources dominated EC at IAP and PG in winter and summer, with contributions of 45.9–71.7 % at IAP and 48.2–76.6 % at PG. The fossil sources of OC contribute 34.7–75.0 % and 39.3–66.9 % for IAP and PG with non-fossil fractions of OC elevated in summer. An extended Gelencsér method using the ¹⁴C measurements was applied for the first time to estimate fossil and non-fossil sources of primary and secondary OC, as well as OC from biomass burning and cooking (POC_f, SOC_f, POC_{nf}, SOC_{nf}, OC_{bb} and OC_{ck}, respectively). Fossil-derived POC is the major contributor during winter and summer at both sites. Fossil-derived SOC contributed more in winter especially at the urban site, with average



435 contributions (to OC) of 32.0 ± 12.5 % and 25.2 ± 7.6 % for IAP, 25.2 ± 10.4 % and 21.1 ± 14.4 % for PG in winter and
summer, respectively. The contribution of SOC_{nf} increased in summer, which is probably associated with formation from
biogenic emissions. A study of relationships among levoglucosan, mannosan and galactosan showed that biomass burning
was mainly from softwood combustion and straw burning. The extended Gelencsér method using ^{14}C data provided a more
robust calculation of OC_{bb} . The contributions of OC_{bb} to OC were 10.6 ± 1.7 % and 10.4 ± 1.5 % for IAP and PG in winter,
6.5 ± 5.2 % and 17.9 ± 3.5 % for IAP and PG in summer. Correlations among WINSOC, WSOC and POC, SOC showed that
440 WINSOC_{f} and $\text{WINSOC}_{\text{nf}}$ were the main components of POC_{f} and POC_{nf} , respectively. However, large fractions of
WINSOC were found in both SOC_{f} and SOC_{nf} especially at the rural site, and the contributions of water-insoluble OC
decreased from winter to summer, with more WSOC formed under favourable conditions in summer. Although derived from
a limited number of samples, our study reflected the different formation mechanisms of SOC between winter and summer,
and between the urban and rural area. It also confirms the feasibility of a new approach of direct source apportionment of
445 carbonaceous aerosol, which was found to compare generally well with the commonly used Chemical Mass Balance and
AMS/ACSM-PMF methods.

Data accessibility

Data supporting this publication are openly available from the UBIRA eData repository at
450 <https://doi.org/10.25500/edata.bham.00000572>.

Author contribution

Z.S. and R.M.H. conceived the research. T.V.V. and D.L. conducted the aerosol sampling and laboratory-based OC/EC
analyses. D.L. and L.J.L. carried out the GC-MS analysis. P.Q.F. supervised GC-MS laboratory work. A.V., V.M. and G.S.
carried out the ^{14}C analysis. S.S. and A.S.H.P. supervised the ^{14}C analysis. X.W. and J.X. conducted the CMB modelling at
455 PG and IAP sites, respectively. S.H. conducted the analysis of the extended Gelencsér (EG) method incorporating ^{14}C data.
Y.S. provided the AMS-PMF data. S.H. and D.L. drafted the paper.

Competing interests

The authors have no conflict of interests.

Special issue statement

460 This article is part of the special issue “In-depth study of air pollution sources and processes within Beijing and its
surrounding region (APHH-Beijing) (ACP/AMT inter-journal SI)”. It is not associated with a conference.



Acknowledgements

This research was funded by the Natural Environment Research Council (Grant No: NE/N007190/1, NE/R005281/1). We thank Bill Bloss, Leigh Crilley, Louisa Kramer from the University of Birmingham, Siyao Yue, Liangfang Wei, Hong Ren, 465 Qiaorong Xie, Wanyu Zhao, Linjie Li, Ping Li, Shengjie Hou, Qingqing Wang, Pingqing Fu and Yele Sun from Institute of Atmospheric Physics, Rachel Dunmore, Ally Lewis, Jacqui Hamilton and James Lee from the University of York, Kebin He and Xiaoting Cheng from Tsinghua University, and James Allan and Hugh Coe from the University of Manchester, Yiqun Han, Hanbing Zhang from King's College London, and Tong Zhu from Peking University for providing logistic and scientific support for the field campaigns. PQF acknowledges funding from the Royal Society – NSFC Advanced Newton 470 Fellowship (NAF\R1\191220).

References

- Abdullahi, K. L., Delgado-Saborit, J. M., and Harrison, R. M.: Sensitivity of a Chemical Mass Balance model for PM_{2.5} to source profiles for differing styles of cooking, *Atmos. Environ.*, 178, 282-285, <https://doi.org/10.1016/j.atmosenv.2018.01.046>, 2018.
- 475 Agrios, K., Salazar, G., Zhang, Y.-L., Uglietti, C., Battaglia, M., Luginbühl, M., Ciobanu, V. G., Vonwiller, M., Szidat, S.: Online coupling of pure O₂ thermo-optical methods – ¹⁴C AMS for source apportionment of carbonaceous aerosols, *Nucl. Instrum. Methods Phys. Res., B*, 361, 288-293, <https://doi.org/10.1016/j.nimb.2015.06.008>, 2015.
- Andreae, M. O., and Merlet, P.: Emission of trace gases and aerosols from biomass burning, *Glob. Biogeochem. Cycles*, 15, 955-966, <https://doi.org/10.1029/2000GB001382>, 2001.
- 480 Barrett, T. E., Robinson, E. M., Usenko, S., and Sheesley, R. J.: Source contributions to wintertime elemental and organic carbon in the Western Arctic based on radiocarbon and tracer apportionment, *Environ. Sci. Technol.*, 49, 11631-11639., <https://doi.org/10.1021/acs.est.5b03081>, 2015
- Bernardoni, V., Calzolari, G., Chiari, M., Fedi, M., Lucarelli, F., Nava, S., Piazzalunga, A., Riccobono, F., Taccetti, F., Valli, G., and Vecchi, R.: Radiocarbon analysis on organic and elemental carbon in aerosol samples and source apportionment at 485 an urban site in Northern Italy, *J. Aerosol Sci.*, 56, 88-99, <https://doi.org/10.1016/j.jaerosci.2012.06.001>, 2013.
- Cai, T., Zhang, Y., Fang, D., Shang, J., Zhan, Y., and Zhang, Y.: Chinese vehicle emissions characteristic testing with small sample size: Results and comparison, *Atmos. Pollut. Res.*, 8, 154-163, <https://doi.org/10.1016/j.apr.2016.08.007>, 2017.
- Castro, L., Pio, C., Harrison, R. M., and Smith, D.: Carbonaceous aerosol in urban and rural European atmospheres: Estimation of secondary organic carbon concentrations, *Atmos. Environ.*, 33, 2771-2781, [https://doi.org/10.1016/S1352-4902310\(98\)00331-8](https://doi.org/10.1016/S1352-4902310(98)00331-8), 1999.



- Chen, J. M., Li, C. L., Ristovski, Z., Milic, A., Gu, Y. T., Islam, M. S., Wang, S. X., Hao, J. M., Zhang, H. F., He, C. R., Guo, H., Fu, H. B., Miljevic, B., Morawska, L., Thai, P., Fat, L., Pereira, G., Ding, A. J., Huang, X., and Dumka, U. C.: A review of biomass burning: Emissions and impacts on air quality, health and climate in China, *Sci. Tot. Environ.*, 579, 1000-1034, <https://doi.org/10.1016/j.scitotenv.2016.11.025>, 2017.
- 495 Chen, H. Y., Yin, S. S., Li, X., Wang, J., and Zhang, R. Q.: Analyses of biomass burning contribution to aerosol in Zhengzhou during wheat harvest season in 2015, *Atmos. Res.*, 207, 62-73, <https://doi.org/10.1016/j.atmosres.2018.02.025>, 2018.
- Cheng, Y., Engling, G., He, K.-B., Duan, F.-K., Ma, Y.L., Du, Z.-Y., Liu, J.-M., Zheng, M., and Weber, R. J.: Biomass burning contribution to Beijing aerosol, *Atmos. Chem. Phys.*, 13, 7765-7781, <https://doi.org/10.5194/acp-13-7765-2013>,
500 2013.
- Chow, J. C., Watson, J. G., Lu, Z., Lowenthal, D. H., Frazier, C. A., Solomon, P. A., Thuillier, R. H., and Magliano, K.: Descriptive analysis of PM_{2.5} and PM₁₀ at regionally representative locations during SJVAQS/AUSPEX, *Atmos. Environ.*, 30, 2079-2112, [https://doi.org/10.1016/1352-2310\(95\)00402-5](https://doi.org/10.1016/1352-2310(95)00402-5), 1996.
- Chow, J. C., Watson, J. G., Crow, D., Lowenthal, D. H., and Murrifield, T.: Comparison of IMPROVE and NIOSH carbon
505 measurements, *Aerosol Sci. Technol.*, 34, 23-34, <https://doi.org/10.1080/02786820119073>, 2001.
- Donahue, N. M., Robinson, A. L., Stanier, C. O., and Pandis, S. N.: Coupled Partitioning, Dilution, and Chemical Aging of Semivolatile Organics, *Environ. Sci. Technol.*, 40, 2635-2643, <https://doi.org/10.1021/es052297c>, 2006.
- Favez, O., Sciare, J., Cachier, H., Alfaro, S. C., and Abdelwahab, M. M.: Significant formation of water-insoluble secondary organic aerosols in semi-arid urban environment, *Geophysical Research Letters*, 35, 5, 10.
510 <https://doi.org/1029/2008gl034446>, 2008.
- Fu, P. Q., Kawamura, K., Chen, J., Li, J., Sun, Y. L., Liu, Y., Tachibana, E., Aggarwal, S. G., Okuzawa, K., Tanimoto, H., Kanaya, Y., and Wang, Z. F.: Diurnal variations of organic molecular tracers and stable carbon isotopic composition in atmospheric aerosols over Mt. Tai in the North China Plain: an influence of biomass burning, *Atmos. Chem. Phys.*, 12, 8359-8375, <https://doi.org/10.5194/acp-12-8359-2012>, 2012.
- 515 Fu, P. Q., Zhuang, G. S., Sun, Y. L., Wang, Q. Z., Chen, J., Ren, L. J., Yang, F., Wang, Z. F., Pan, X. L., Li, X. D., and Kawamura, K.: Molecular markers of biomass burning, fungal spores and biogenic SOA in the Taklimakan desert aerosols, *Atmos. Environ.*, 130, 64-73, <https://doi.org/10.1016/j.atmosenv.2015.10.087>, 2016.
- Gelencsér, A., May, B., Simpson, D., Sánchez-Ochoa, A., Kasper-Giebl, A., Puxbaum, H., Caseiro, A., Pio, C., and Legrand, M.: Source apportionment of PM_{2.5} organic aerosol over Europe: Primary/secondary, natural/anthropogenic, and
520 fossil/biogenic origin, *J. Geophys. Res.: Atmospheres*, 112, D23S04, <https://doi.org/10.1029/2006JD008094>, 2007.
- Gray, H. A., and Cass, G. R.: Source contributions to atmospheric fine carbon particle concentrations, *Atmos. Environ.*, 32, 3805-3825, [https://doi.org/10.1016/S1352-2310\(97\)00446-9](https://doi.org/10.1016/S1352-2310(97)00446-9), 1998.



- Han, Y. M., Chen, L.-W.A., Huang, R.-J., Chow, J. C., Watson, J. G., Ni, H. Y., Liu, S. X., Fung, K. K., Shen, Z. X., Wei, C., Wang, Q. Y., Tian, J., Zhao, Z. Z., Prévôt, A. S. H., and Cao, J. J.: Carbonaceous aerosols in megacity Xi'an, China: Implications of thermal/optical protocols comparison, *Atmos. Environ.*, 132, 58-68, <https://doi.org/10.1016/j.atmosenv.2016.02.023>, 2016.
- 525 He, K., Yang, F., Ma, Y., Zhang, Q., Yao, X., Chan, C. K., Cadle, S., Chan, T., and Mulawa, P.: The characteristics of PM_{2.5} in Beijing, China, *Atmos. Environ.*, 35, 4959-4970, [https://doi.org/10.1016/S1352-2310\(01\)00301-6](https://doi.org/10.1016/S1352-2310(01)00301-6), 2001.
- Hou, B.-D., Tang, X., Ma, C., Liu, L., Wei, Y.-M., Liao, H.: Cooking fuel choice in rural China: results from microdata, *J. Clean. Prod.*, 142, 538-547, <https://doi.org/10.1016/j.jclepro.2016.05.031>, 2017.
- 530 Huang, R.-J., Zhang, Y., Bozzetti, C., Ho, K.-F., Cao, J.-J., Han, Y., Daellenbach, K. R., Slowik, J. G., Platt, S. M., Canonaco, F., Zotter, P., Wolf, R., Pieber, S. M., Bruns, E. A., Crippa, M., Ciarelli, G., Piazzalunga, A., Schwikowski, M., Abbazade, G., Schnelle-Kreis, J., Zimmermann, R., An, Z., Szidat, S., Baltensperger, U., Haddad, I. E., and Prévôt, A. S. H.: High secondary aerosol contribution to particulate pollution during haze events in China, *Nature*, 514, 218-222, <https://doi.org/10.1038/nature13774>, 2014.
- Jimenez, J. L., Canagaratna, M. R., Donahue, N. M., Prevot, A. S. H., Zhang, Q., Kroll, J. H., DeCarlo, P. F., Allan, J. D., Coe, H., Ng, N. L., Aiken, A. C., Docherty, K. S., Ulbrich, I. M., Grieshop, A. P., Robinson, A. L., Duplissy, J., Smith, J. D., Wilson, K. R., Lanz, V. A., Hueglin, C., Sun, Y. L., Tian, J., Laaksonen, A., Raatikainen, T., Rautiainen, J., Vaattovaara, P., Ehn, M., Kulmala, M., Tomlinson, J. M., Collins, D. R., Cubison, M. J., Dunlea, E. J., Huffman, J. A., Onasch, T. B., Alfarra, M. R., Williams, P. I., Bower, K., Kondo, Y., Schneider, J., Drewnick, F., Borrmann, S., Weimer, S., Demerjian, K., Salcedo, D., Cottrell, L., Griffin, R., Takami, A., Miyoshi, T., Hatakeyama, S., Shimono, A., Sun, J. Y., Zhang, Y. M., Dzepina, K., Kimmel, J. R., Sueper, D., Jayne, J. T., Herndon, S. C., Trimborn, A. M., Williams, L. R., Wood, E. C., Middlebrook, A. M., Kolb, C. E., Baltensperger, U., and Worsnop, D. R.: Evolution of organic aerosols in the atmosphere, *Science* 326, 1525-1529, <https://doi.org/10.1126/science.1180353>, 2009.
- 540 Kang, M., Ren, L., Ren, H., Zhao, Y., Kawamura, K., Zhang, H., Wei, L., Sun, Y., Wang, Z., and Fu, P.: Primary biogenic and anthropogenic sources of organic aerosols in Beijing, China: Insights from saccharides and n-alkanes, *Environ. Pollut.*, 243, 1579-1587, <https://doi.org/10.1016/j.envpol.2018.09.118>, 2018.
- Kawamura, K., Izawa, Y., Mochida, M., and Shiraiwa, T.: Ice core records of biomass burning tracers (levoglucosan and dehydroabietic, vanillic and p-hydroxybenzoic acids) and total organic carbon for past 300 years in the Kamchatka Peninsula, Northeast Asia, *Geochim. Cosmochim. Acta* 99, 317-329, <https://doi.org/10.1016/j.gca.2012.08.006>, 2012.
- 550 Levin, I., Naegler, T., Kromer, B., Diehl, M., Francey, R., Gomez-Pelaez, A., Steele, P., Wagenbach, D., Weller, R., and Worthy, D.: Observations and modelling of the global distribution and long-term trend of atmospheric ¹⁴CO₂, *Tellus B: Chem. Phys. Meteorol.*, 62, 26-46, <https://doi.org/10.1111/j.1600-0889.2009.00446.x>, 2010.



- Lewis, C. W., Klouda, G. A., and Ellenson W. D.: Radiocarbon measurement of the biogenic contribution to summertime
555 PM_{2.5} ambient aerosol in Nashville, TN, *Atmos. Environ.*, 38, 6053-6061, <https://doi.org/10.1080/02786820500521007>,
2004.
- Li, L. J., Ren, L. J., Ren, H., Yue, S. Y., Xie, Q. R., Zhao, W. Y., Kang, M. J., Li, J., Wang, Z. F., Sun, Y. L., and Fu, P. Q.:
Molecular Characterization and Seasonal Variation in Primary and Secondary Organic Aerosols in Beijing, China, *J.*
Geophys. Res. Atmospheres, 123, 12394-12412, <https://doi.org/10.1029/2018JD028527>, 2018.
- 560 Li, X., Chen, M., Le, H. P., Wang, F., Guo, Z., Iinuma, Y., Chen, J., and Herrmann, H.: Atmospheric outflow of PM_{2.5}
saccharides from megacity Shanghai to East China Sea: Impact of biological and biomass burning sources, *Atmos. Environ.*,
143, 1-14, <https://doi.org/10.1016/j.atmosenv.2016.08.039>, 2016.
- Liu, D., Li, J., Zhang, Y. L., Xu, Y., Liu, X., Ding, P., Shen, C. D., Chen, Y. J., Tian, C. G., and Zhang, G.: The use of
levoglucosan and radiocarbon for source apportionment of PM_{2.5} carbonaceous aerosols at a background site in east China,
565 *Environ. Sci. Technol.*, 47, 10454-10461, <https://doi.org/10.1021/es401250k>, 2013.
- Liu, J. W., Mo, Y. Z., Li, J., Liu, D., Shen, C. D., Ding, P., Jiang, H. Y., Cheng, Z. N., Zhang, X. Y., Tian, C. G., Chen, Y.
J., and Zhang, G.: Radiocarbon-derived source apportionment of fine carbonaceous aerosols before, during, and after the
2014 Asia-Pacific Economic Cooperation (APEC) summit in Beijing, China, *J. Geophys. Res., Atmospheres* 121, 4177-
4187, <https://doi.org/10.1002/2016JD024865>, 2016a.
- 570 Liu, J. W., Li, J., Vonwiller, M., Liu, D., Cheng, H. R., Shen, K. J., Salazar, G., Agrios, K., Zhang, Y. L., He, Q. F., Ding,
X., Zhong, G. C., Wang, X. M., Szidat, S., and Zhang, G.: The importance of non-fossil sources in carbonaceous aerosols in
a megacity of central China during the 2013 winter haze episode: A source apportionment constrained by radiocarbon and
organic tracers, *Atmos. Environ.*, 144, 60-68, <https://doi.org/10.1016/j.atmosenv.2016.08.068>, 2016b.
- Liu, D., Li, J., Cheng, Z. N., Zhong, G. C., Zhu, S. Y., Ding, P., Shen, C. D., Tian, C. G., Chen, Y. J., Zhi, G. R., and Zhang,
575 G.: Sources of non-fossil-fuel emissions in carbonaceous aerosols during early winter in Chinese cities, *Atmos. Chem.*
Phys., 17, 11491-11502, <https://doi.org/10.5194/acp-17-11491-2017>, 2017.
- Liu, D., Vonwiller, M., Li, J., Liu, J., Szidat, S., Zhang, Y., Tian, C., Chen, Y., Cheng, Z., Zhong, G., Fu, P., and Zhang, G.:
Fossil and non-fossil fuel sources of organic and elemental carbon aerosols in Beijing, Shanghai and Guangzhou: Seasonal
carbon-source variation, *Aerosol Air Qual. Res.*, 20, <https://doi.org/10.4209/aaqr.2019.12.0642>, 2020.
- 580 Minguillón, M. C., Perron, N., Querol, X., Szidat, S., Fahrni, S. M., Alastuey, A., Jimenez, J. L., Mohr, C., Ortega, A. M.,
Day, D. A., Lanz, V. A., Wacker, L., Reche, C., Cusack, M., Amato, F., Kiss, G., Hoffer, A., Decesari, S., Moretti, F.,
Hillamo, R., Teinilä, K., Seco, R., Peñuela, J., Metzger, A., Schallhart, S., Müller, M., Hansel, A., Burkhardt, J. F.,
Baltensperger, U., and Prévôt, A. S. H.: Fossil versus contemporary sources of fine elemental and organic carbonaceous
particulate matter during the DAURE campaign in Northeast Spain, *Atmos. Chem. Phys.* 11, 12067-12084,
585 <https://doi.org/10.5194/acp-11-12067-2011>, 2011.



- Miyazaki, Y., Kondo, Y., Takegawa, N., Komazaki, Y., Fukuda, M., Kawamura, K., Mochida, M., Okuzawa, K., and Weber, R. J.: Time-resolved measurements of water-soluble organic carbon in Tokyo, *J. Geophys. Res., Atmospheres*, 111, D23206, <https://doi.org/10.1029/2006JD007125>, 2006.
- Ng, N. L., Herndon, S. C., Trimborn, A., Canagaratna, M. R., Croteau, P. L., Onasch, T.B., Sueper, D., Worsnop, D. R.,
590 Zhang, Q., Sun, Y. L., and Jayne, J. T.: An aerosol chemical speciation monitor (ACSM) for routine monitoring of the composition and mass concentrations of ambient aerosol, *Aerosol Sci. Technol.*, 45, 780-794, <https://doi.org/10.1080/02786826.2011.560211>, 2011.
- Ni, H. Y., Huang, R.-J., Cao, J. J., Liu, W. G., Zhang, T., Wang, M., Meijer, H. A. J., and Dusek, U.: Source apportionment of carbonaceous aerosols in Xi'an, China: insights from a full year of measurements of radiocarbon and the stable isotope
595 ^{13}C , *Atmos. Chem. Phys.*, 18, 16,363-16,383, <https://doi.org/10.5194/acp-18-16363-2018>, 2018.
- Paatero, P., and Tapper, U.: Positive matrix factorization - a nonnegative factor model with optimal utilization of error estimates of data values, *Environmetrics*, 5, <https://doi.org/111-126>, 10.1002/env.3170050203, 1994.
- Palstra, S. W. L., and Meijer, H. A. J.: Biogenic carbon fraction of biogas and natural gas fuel mixtures determined with ^{14}C , *Radiocarbon*, 56, 7-28, <https://doi.org/10.2458/56.16514>, 2014.
- 600 Paraskevopoulou, D., Liakakou, E., Gerasopoulos, E., Theodosi, C., and Mihalopoulos, N.: Long-term characterization of organic and elemental carbon in the $\text{PM}_{2.5}$ fraction: the case of Athens, Greece, *Atmos. Chem. Phys.* 14, 13313-13,325, <https://doi.org/10.5194/acp-14-13313-2014>, 2014.
- Pavuluri, C. M., Kawamura, K., Uchida, M., Kondo, M., and Fu, P. Q.: Enhanced modern carbon and biogenic organic tracers in Northeast Asian aerosols during spring/summer, *J. Geophys. Res., Atmospheres*, 118, 2362-2371,
605 <https://doi.org/10.1002/jgrd.50244>, 2013.
- Puxbaum, H., Caseiro, A., Sánchez-Ochoa, A., Kasper-Giebl, A., Claeys, M., Gelencsér, A., Legrand, M., Preunkert, S., and Pio, C.: Levoglucosan levels at background sites in Europe for assessing the impact of biomass combustion on the European aerosol background. *J. Geophys. Res., Atmospheres*, 112(D23), <https://doi.org/10.1029/2006JD008114>, 2007.
- Reyes-Villegas, E., Bannan, T., Le Breton, M., Mehra, A., Priestley, M., Percival, C., Coe, H., and Allan, J. D.: Online
610 chemical characterization of food-cooking organic aerosols: Implications for source apportionment, *Environ. Sci. Technol.*, 52, 5308-5318, <https://doi.org/10.1021/acs.est.7b06278>, 2018.
- Robinson, A. L., Donahue, N. M., Shrivastava, M. K., Weitkamp, E. A., Sage, A. M., Grieshop, A. P., Lane, T. E., Pierce, J. R., and Pandis, S. N.: Rethinking organic aerosols: Semivolatile emissions and photochemical aging, *Science*, 315, 1259-1262, <https://doi.org/10.1126/science.1133061>, 2007.
- 615 Rogge, W. F., Hildemann, L. M., Mazurek, M. A., Cass, G. R., and Simoneit, B. R. T.: Sources of fine organic aerosol. 4. Particulate abrasion products from leaf surfaces of urban plants, *Environ. Sci. Technol.*, 27, 2700-2711, <https://doi.org/10.1021/es00049a008>, 1993.



- Salma, I., Nemeth, Z., Weidinger, T., Maenhaut, W., Claeys, M., Molnar, M., Major, I., Ajtai, T., Utry, N., and Bozoki, Z.: Source apportionment of carbonaceous chemical species to fossil fuel combustion, biomass burning and biogenic emissions by a coupled radiocarbon-levoglucosan marker method, *Atmos. Chem. Phys.*, 17, 13767-13781, <https://doi.org/10.5194/acp-17-13767-2017>, 2017.
- Sciare, J., d'Argouges, O., Sarda-Esteve, R., Gaimoz, C., Dolgorouky, C., Bonnaire, N., Favez, O., Bonsang, B., and Gros, V.: Large contribution of water-insoluble secondary organic aerosols in the region of Paris (France) during wintertime, *J. Geophys. Res.-Atmos.*, 116, 24, <https://doi.org/10.1029/2011jd015756>, 2011.
- Shi, Z., Vu, T., Kotthaus, S., Harrison, R. M., Grimmond, S., Yue, S., Zhu, T., Lee, J., Han, Y., Demuzere, M., Dunmore, R.E., Ren, L., Liu, D., Wang, Y., Wild, O., Allan, J., Acton, W. J., Barlow, J., Barratt, B., Beddows, D., Bloss, W. J., Calzolari, G., Carruthers, D., Carslaw, D. C., Chan, Q., Chatzidiakou, L., Chen, Y., Crilley, L., Coe, H., Dai, T., Doherty, R., Duan, F., Fu, P., Ge, B., Ge, M., Guan, D., Hamilton, J. F., He, K., Heal, M., Heard, D., Hewitt, C. N., Hollaway, M., Hu, M., Ji, D., Jiang, X., Jones, R., Kalberer, M., Kelly, F. J., Kramer, L., Langford, B., Lin, C., Lewis, A. C., Li, J., Li, W., Liu, H., Liu, J., Loh, M., Lu, K., Lucarelli, F., Mann, G., McFiggans, G., Miller, M. R., Mills, G., Monk, P., Nemitz, E., O'Connor, F., Ouyang, B., Palmer, P. I., Percival, C., Popoola, O., Reeves, C., Rickard, A. R., Shao, L., Shi, G., Spracklen, D., Stevenson, D., Sun, Y., Sun, Z., Tao, S., Tong, S., Wang, Q., Wang, W., Wang, X., Wang, X., Wang, Z., Wei, L., Whalley, L., Wu, X., Wu, Z., Xie, P., Yang, F., Zhang, Q., Zhang, Y., Zhang, Y., and Zheng, M.: Introduction to the special issue "In-depth study of air pollution sources and processes within Beijing and its surrounding region (APHH-Beijing)", *Atmos. Chem. Phys.*, 19, 7519-7546, <https://doi.org/10.5194/acp-19-7519-2019>, 2019.
- Simoneit, B. R. T., Schauer, J. J., Nolte, C. G., Oros, D. R., Elias, V. O., Fraser, M. P., Rogge, W. F., Cass, G. R.: Levoglucosan, a tracer for cellulose in biomass burning and atmospheric particles, *Atmos. Environ.* 33, 173-182, [https://doi.org/10.1016/S1352-2310\(98\)00145-9](https://doi.org/10.1016/S1352-2310(98)00145-9), 1999.
- Song, Y., Tang, X., Xie, S., Zhang, Y., Wei, Y., Zhang, M., Zeng, L., and Lu S.: Source apportionment of PM_{2.5} in Beijing in 2004, *J. Hazard. Mater.* 146, 124-130, <https://doi.org/10.1016/j.jhazmat.2006.11.058>, 2007.
- Sullivan, A. P., Guo, H., Schroder, J. C., Campuzano-Jost, P., Jimenez, J. L., Campos, T., Shah, V., Jaegle, L., Lee, B. H., Lopez-Hilfiker, F. D., Thornton, J. A., Brown, S. S., and Weber, R. J.: Biomass burning markers and residential burning in the WINTER aircraft campaign, *J. Geophys. Res., Atmospheres*, 124, 1846-1861, <https://doi.org/10.1029/2017JD028153>, 2019.
- Sun, Y., Jiang, Q., Xu, Y., Ma, Y., Zhang, Y., Liu, X., Li, W., Wang, F., Li, J., Wang, P., and Li, Z.: Aerosol characterization over the North China Plain: Haze life cycle and biomass burning impacts in summer, *J. Geophys. Res., Atmospheres*, 121, 2508-2521, <https://doi.org/10.1002/2015JD024261>, 2016.
- Sun, J., Shen, Z. X., Zhang, Y., Zhang, Q., Lei, Y. L., Huang, Y., Niu, X. Y., Xu, H. M., Cao, J. J., Ho, S. S. H., and Li, X. X.: Characterization of PM_{2.5} source profiles from typical biomass burning of maize straw, wheat straw, wood branch, and



- 650 their processed products (briquette and charcoal) in China, *Atmos. Environ.*, 205, 36-45,
<https://doi.org/10.1016/j.atmosenv.2019.02.038>, 2019a.
- Sun, J., Shen, Z. X., Zhang, Y., Zhang, Q., Wang, F. R., Wang, T., Chang, X. J., Lei, Y. L., Xu, H. M., Cao, J. J., Zhang, N.
N., Liu, S. X., and Li, X. X.: Effects of biomass briquetting and carbonization on PM_{2.5} emission from residential burning in
Guangzhong Plain, China. *Fuel*, 244, 379-387, <https://doi.org/10.1016/j.fuel.2019.02.031>, 2019b.
- 655 Sun, Y., He, Y., Kuang, Y., Xu, W., Song, S., Ma, N., Tao, J., Cheng, P., Wu, C., Su, H., Cheng, Y., Xie, C., Chen, C., Lei,
L., Qiu, Y., Fu, P., Croteau, P., and Worsnop, D. R.: Chemical differences between PM₁ and PM_{2.5} in highly polluted
environment and implications in air pollution studies, *Geophys. Res. Lett.*, 47, e2019GL086288.
<https://doi.org/10.1029/2019GL086288>, 2020.
- Szidat, S., Jenk, T. M., Gäggeler, H. W., Synal, H.-A.: Source apportionment of aerosols by ¹⁴C measurements in different
660 carbonaceous particle fractions, *Radiocarbon* 46, 475-484, <https://doi.org/10.1017/S0033822200039783.2004>.
- Szidat, S., Jenk, T. M., Synal, H.-A., Kalberer, M., Wacker, L., Hajdas, I., Kasper-Giebl, A., Baltensperger, U.:
Contributions of fossil fuel, biomass-burning, and biogenic emissions to carbonaceous aerosols in Zurich as traced by ¹⁴C, *J.*
Geophys. Res., Atmospheres, 111, D07206, <https://doi.org/10.1029/2005JD006590>, 2006.
- Szidat, S., Ruff, M., Perron, N., Wacker, L., Synal, H.-A., Hallquist, M., Shannigrahi, A. S., Yttri, K. E., Dye, C., and
665 Simpson, D.: Fossil and non-fossil sources of organic carbon (OC) and elemental carbon (EC) in Göteborg, Sweden, *Atmos.*
Chem. Phys., 9, 1521-1535, <https://doi.org/10.5194/acp-9-1521-2009>, 2009.
- Szidat, S., Salazar, G. A., Vogel, E., Battaglia, M., Wacker, L., Synal, H.-A., and Türler, A.: ¹⁴C analysis and sample
preparation at the new bern laboratory for the analysis of radiocarbon with AMS (LARA), *Radiocarbon*, 56, 561-566,
<https://doi.org/10.2458/56.17457>, 2014.
- 670 Ulbrich, I. M., Canagaratna, M. R., Zhang, Q., Worsnop, D. R., and Jimenez, J. L.: Interpretation of organic components
from Positive Matrix Factorization of aerosol mass spectrometric data, *Atmos. Chem. Phys.*, 9, 2891-2918,
<https://doi.org/10.5194/acp-9-2891-2009>, 2009.
- Vlachou, A., Daellenbach, K. R., Bozzetti, C., Chazeanu, B., Salazar, G. A., Szidat, S., Jaffrezo, J.-L., Hueglin, C.,
Baltensperger, U., El Haddad, I., and Prévôt, A. S. H.: Advanced source apportionment of carbonaceous aerosols by
675 coupling offline AMS and radiocarbon size-segregated measurements over a nearly 2-year period, *Atmos. Chem. Phys.*, 18,
6187-6206, <https://doi.org/10.5194/acp-18-6187-2018>, 2018.
- Wang, Q., Shao, M., Zhang, Y., Wei, Y., Hu, M., and Guo, S.: Source apportionment of fine organic aerosols in Beijing,
Atmos. Chem. Phys. 9, 8573-8585, <https://doi.org/10.5194/acp-9-8573-2009>, 2009.
- Wu, X., Chen, C., Vu, T. V., Liu, D., Baldo, C., Shen, X., Zhang, Q., Cen, K., Zheng, M., He, K., Shi, Z., and Harrison, R.
680 M.: Source apportionment of fine organic carbon (OC) using receptor modelling at a rural site of Beijing: Insight into



- seasonal and diurnal variation of source contributions, *Environ. Pollut.*, 115078, <https://doi.org/10.1016/j.envpol.2020.115078>, 2020.
- Xu, J., Song, S., Harrison, R. M., Song, C., Wei, L., Zhang, Q., Sun, Y., Lei, L., Zhang, C., Yao, X., Chen, D., Li, W., Wu, M., Tian, H., Luo, L., Tong, S., Li, W., Wang, J., Shi, G., Huangfu, Y., Tian, Y., Ge, B., Su, S., Peng, C., Chen, Y., Yang, F., Mihajlidi-Zelić, A., Đorđević, D., Swift, S. J., Andrews, I., Hamilton, J. F., Sun, Y., Kramawijaya, A., Han, J., Saksakulkrai, S., Baldo, C., Hou, S., Zheng, F., Daellenbach, K. R., Yan, C., Liu, Y., Kulmala, M., Fu, P., and Shi, Z.: An inter-laboratory comparison of aerosol inorganic ion measurements by Ion Chromatography: implications for aerosol pH estimate, *Atmos. Meas. Tech. Discuss.*, 2020, 1-36, <https://doi.org/10.5194/amt-2020-156>, 2020a.
- Xu, J., Wu, X., Vu, T. V., Liu, D., Zhang, Y., Shi, Z., and Harrison, R. M.: Source apportionment of fine aerosols applying chemical mass balance (CMB) model at an urban site of Beijing, (under preparation), 2020b.
- Xu, W., Sun, Y., Wang, Q., Zhao, J., Wang, J., Ge, X., Xie, C., Zhou, W., Du, W., Li, J., Fu, P., Wang, Z., Worsnop, D. R., Coe, H.: Changes in aerosol chemistry from 2014 to 2016 in winter in Beijing: insights from high-resolution aerosol mass spectrometry, *J. Geophys. Res., Atmospheres*, 124, 1132-1147, <https://doi.org/10.1029/2018JD029245>, 2019.
- Yan, X., Ohara, T., and Akimoto, H.: Bottom-up estimate of biomass burning in mainland China, *Atmos. Environ.*, 40, 5262-5273, <https://doi.org/10.1016/j.atmosenv.2006.04.040>, 2006.
- Yan, C., Zheng, M., Sullivan, A. P., Shen, G., Chen, Y., Wang, S., Zhao, B., Cai, S., Desyaterik, Y., X. Li, Zhou, T., Ö. Gustafsson, and Collett Jr., J. L.: Residential coal combustion as a source of levoglucosan in China, *Environ. Sci. Technol.*, 52, 1665-1674, <https://doi.org/10.1021/acs.est.7b05858>, 2018.
- Yan, C. Q., Sullivan, A. P., Cheng, Y., Zheng, M., Zhang, Y. H., Zhu, T., and Collett, J. L.: Characterization of saccharides and associated usage in determining biogenic and biomass burning aerosols in atmospheric fine particulate matter in the North China Plain, *Sci. Tot. Environ.*, 650, 2939-2950, <https://doi.org/10.1016/j.scitotenv.2018.09.325>, 2019.
- Yang, F., Kawamura, K., Chen, J., Ho, K., Lee, S., Gao, Y., Cui, L., Wang, T., and Fu, P.: Anthropogenic and biogenic organic compounds in summertime fine aerosols (PM_{2.5}) in Beijing, China, *Atmos. Environ.*, 124, 166-175, <https://doi.org/10.1016/j.atmosenv.2015.08.095>, 2016.
- Yin, J., Harrison, R. M., Chen, Q., Rutter, A., and Schauer, J. J.: Source apportionment of fine particles at urban background and rural sites in the UK atmosphere, *Atmos. Environ.*, 44, 841-851, <https://doi.org/10.1016/j.atmosenv.2009.11.026>, 2010.
- Yin, J., Cumberland, S. A., Harrison, R. M., Allan, J., Young, D. E., Williams, P. I., and Coe, H.: Receptor modelling of fine particles in southern England using CMB including comparison with AMS-PMF factors, *Atmos. Chem. Phys.*, 15, 2139-2158, <https://doi.org/10.5194/acp-15-2139-2015>, 2015.
- Yttri, K. E., Simpson, D., Stenström, K., Puxbaum, H., and Svendby, T.: Source apportionment of the carbonaceous aerosol in Norway - quantitative estimates based on ¹⁴C, thermal-optical and organic tracer analysis, *Atmos. Chem. Phys.*, 11, 9375-9394, <https://doi.org/10.5194/acp-11-9375-2011>, 2011.



- Zdráhal, Z., Oliveira, J., Vermeylen, R., Claeys, M., and Maenhaut W.: Improved method for quantifying levoglucosan and related monosaccharide anhydrides in atmospheric aerosols and application to samples from urban and tropical locations, Environ. Sci. Technol., 36, 747-753, <https://doi.org/10.1021/es015619v>, 2002.
- 715 Zhang Y., -X., Shao, M., Zhang, Y.-H., Zeng, L.-M, He, L.-Y, Zhu, B., We, Y.-J., Zhu, X.-L.: Source profiles of particulate organic matters emitted from cereal straw burnings, J. Environ. Sci., 19, 167-175, [https://doi.org/10.1016/S1001-0742\(07\)60027-8](https://doi.org/10.1016/S1001-0742(07)60027-8), 2007.
- Zhang, T., Claeys, M., Cachier, H., Dong, S., Wang, W., Maenhaut, W., and Liu, X.: Identification and estimation of the biomass burning contribution to Beijing aerosol using levoglucosan as a molecular marker, Atmos. Environ., 42, 7013-7021, <https://doi.org/10.1016/j.atmosenv.2008.04.050>, 2008a.
- 720 Zhang, Y. X., Schauer, J. J., Zhang, Y. H., Zeng, L. M., Wei, Y. J., Liu, Y., and Shao, M.: Characteristics of particulate carbon emissions from real-world Chinese coal combustion, Environ. Sci. Technol., 42, 5068-5073, <https://doi.org/10.1021/es7022576>, 2008b.
- 725 Zhang, Y. L., Perron, N., Ciobanu, V. G., Zotter, P., Minguillón, M. C., Wacker, L., Prévôt, A. S. H., Baltensperger, U., and Szidat, S.: On the isolation of OC and EC and the optimal strategy of radiocarbon-based source apportionment of carbonaceous aerosols, Atmos. Chem. Phys, 12, 10,841-10,856, <https://doi.org/10.5194/acp-12-10841-2012>, 2012
- Zhang, Y. L., Huang, R. J., El Haddad, I., Ho, K. F., Cao, J. J., Han, Y., Zotter, P., Bozzetti, C., Daellenbach, K. R., Canonaco, F., Slowik, J. G., Salazar, G., Schwikowski, M., Schnelle-Kreis, J., Abbaszade, G., Zimmermann, R., Baltensperger, U., Prevot, A. S. H., and Szidat, S.: Fossil vs. non-fossil sources of fine carbonaceous aerosols in four Chinese cities during the extreme winter haze episode of 2013, Atmos. Chem. Phys, 15, 1299-1312, <https://doi.org/10.5194/acp-15-1299-2015>, 2015.
- 730 Zhang, Y.-L., Kawamura, K., Agrios, K., Lee, M., Salazar, G., and Szidat, S.: Fossil and nonfossil sources of organic and elemental carbon aerosols in the outflow from Northeast China, Environ. Sci. Technol., 50, 6284-6292, <https://doi.org/10.1021/acs.est.6b00351>, 2016.
- 735 Zhang, Y., Ren, H., Sun, Y., Cao, F., Chang, Y., Liu, S., Lee, X., Agrios, K., Kawamura, K., Liu, D., Ren, L., Du, W., Wang, Z., Prévôt, A. S. H., Szidat, S., and Fu, P.: High contribution of nonfossil sources to submicrometer organic aerosols in Beijing, China, Environ. Sci. Technol., 51, 7842-7852, <https://doi.org/10.1021/acs.est.7b01517>, 2017.
- Zhang, Y.-L., El-Haddad, I., Huang, R.-J., Ho, K.-F., Cao, J.-J. Han, Y., Zotter, P., Bozzetti, C., Daellenbach, K. R., Slowik, J. G., Salazar, G., Prévôt, A. S. H., and Szidat, S.: Large contribution of fossil fuel derived secondary organic carbon to water soluble organic aerosols in winter haze in China, Atmos. Chem. Phys, 18, 4005-4017, <https://doi.org/10.5194/acp-18-4005-2018>, 2018.
- 740 Zhang, X., Hecobian, A., Zheng, M., Frank, N. H., and Weber, R. J.: Biomass burning impact on PM_{2.5} over the southeastern US during 2007: integrating chemically speciated FRM filter measurements, MODIS fire counts and PMF



- 745 analysis, *Atmos. Chem. Phys.*, 10, 6839-6853, <https://doi.org/10.5194/acp-10-6839-2010>, 2010Zhang. X., Lu. Y., Wang. Q., and Qian X.: A high-resolution inventory of air pollutant emissions from crop residue burning in China, *Atmos. Environ.*, 213:207-214, <https://doi.org/10.1016/j.atmosenv.2019.06.009>, 2019.
- Zhao, X., Hu, Q., Wang, X., Ding, X., He, Q., Zhang, Z., Shen, R., Lü, S., Liu, T., Fu, X., and Chen, L.: Composition profiles of organic aerosols from Chinese residential cooking: case study in urban Guangzhou, south China, *J. Atmos. Chem.*, 72, 1-18, <https://doi.org/10.1007/s10874-015-9298-0>, 2015.
- 750 Zhou, Y., Xing, X., Lang, J., Chen, D., Cheng, S., Wei, L., Wei, X., and Liu, C.: A comprehensive biomass burning emission inventory with high spatial and temporal resolution in China, *Atmos. Chem. Phys.*, 17, 2839-2864, <https://doi.org/10.5194/acp-17-2839-2017>, 2017.
- Zhou, W., Wang, Q., Zhao, X., Xu, W., Chen, C., Du, W., Zhao, J., Canonaco, F., Prévôt, A. S. H., Fu, P., Wang, Z., Worsnop, D. R., and Sun, Y.: Characterization and source apportionment of organic aerosol at 260m on a meteorological tower in Beijing, China, *Atmos. Chem. Phys.*, 18, 3951-3968, <https://doi.org/10.5194/acp-18-3951-2018>, 2018.
- 755 Zotter, P., Ciobanu, V. G., Zhang, Y. L., El-Haddad, I., Macchia, M., Daellenbach, K. R., Salazar, G. A., Huang, R.-J., Wacker, L., Hueglin, C., Piazzalunga, A., Fermo, P., Schwikowski, M., Baltensperger, U., Szidat, S., and Prévôt, A. S. H.: Radiocarbon analysis of elemental and organic carbon in Switzerland during winter-smog episodes from 2008 to 2012-Part 1: Source apportionment and spatial variability, *Atmos. Chem. Phys.*, 14, 13551-13570, <https://doi.org/10.5194/acp-14-13551-2014>, 2014.
- 760



TABLE LEGENDS:

Table 1 Equations for ^{14}C -based source apportionment, see Sect. 3.2 for the details.

765 **Table 2** Statistical summary of concentrations, ratios and meteorological parameters at the IAP and PG sites during winter and summer campaigns.

Table 3 Pearson correlations of species at IAP and PG sites.

Table 4 Comparison of LG concentrations and OC from biomass burning in this study and related literature.

Table 5 Source contribution estimates ($\mu\text{g m}^{-3}$) for OC at IAP and PG in winter and summer.

770 FIGURE LEGENDS:

Figure 1 Time series of $\text{PM}_{2.5}$ and its major components at IAP and PG during winter (right) and summer (left).

Figure 2 Time series of concentrations of WSOC_f , WSOC_{nf} , WINSOC_f , WINSOC_{nf} , EC_f and EC_{nf} (left) and their relative contributions to TC (right) at IAP and PG.

775 **Figure 3** Scatter plot of LG/MN vs. LG/GA from different types of biomass burning emissions (Cheng et al., 2013; Sun et al., 2019b; Sun et al., 2019a), including those measured in $\text{PM}_{2.5}$ samples at IAP and PG during winter and summer. The range of LG/MA is 7.66–13.41 and 5.48–22.40 for IAP in winter and summer, 2.45–60.20 and 3.27–17.71 for PG in winter and summer, while the range of LG/GA is 3.98–6.92, 2.78–101.43, 1.97–34.66 and 1.51–13.39, respectively.

780 **Figure 4** Concentrations of OC from softwood (OC_{wood}) vs. OC from straw (OC_{straw}) at IAP (upper) and PG (lower) and variations of OC_{wood} fractions.

Figure 5 Correlations of OC sources from extended Gelencsér method with those from CMB model. EG denotes extended Gelencsér method, (a): primary OC from fossil sources, (b): primary OC from non-fossil sources, (c): secondary OC, (d): OC from biomass burning, (e): OC from cooking, (f): correlations of OC_{ck} from extended Gelencsér method and AMS/ACMS-PMF model (AMS for IAP and ACMS for PG).

785 **Figure 6** Fractions of each source (i.e., POC_f , SOC_f , OC_{bb} , OC_{ck} and SOC_{nf}) in OC based on the extended Gelencsér method. f: fossil fuel sources, nf: non-fossil sources, bb: biomass burning, ck: cooking. The box denotes



the 25th (lower line), 50th (middle line), and 75th (top line) percentiles; the solid squares within the box denote the mean values; the end of the vertical bars represents the 10th (below the box) and 90th (above the box) percentiles; and the solid dots denote maximum and minimum values.

790 **Figure 7**

Correlations of WINSOC, WSOC with POC, SOC at IAP and PG sites in winter and summer. The slopes and correlation coefficients are summarized in Table S5.



Table 1. Equations for ^{14}C -based source apportionment, see Sect. 3.2 for the details.

| | Extended Gelencsér method |
|--------------------------|---|
| EC_{bb} | $\approx \text{EC}_{\text{nf}}$, measured by ^{14}C |
| EC_{f} | measured by ^{14}C |
| OC_{nf} | measured by ^{14}C |
| OC_{f} | measured by ^{14}C |
| POC_{f} | $\text{EC}_{\text{f}} \times (\text{OC}/\text{EC})_{\text{f, min}}$ |
| SOC_{f} | $\text{OC}_{\text{f}} - \text{POC}_{\text{f}}$ |
| POC_{nf} | $\text{EC}_{\text{nf}} \times (\text{OC}/\text{EC})_{\text{nf, min}}$ |
| SOC_{nf} | $\text{OC}_{\text{nf}} - \text{POC}_{\text{nf}}$ |
| OC_{bb} | $\text{EC}_{\text{nf}} \times (\text{OC}/\text{EC})_{\text{bb}} = \text{LG} \times (\text{OC}/\text{LG})_{\text{bb}}$ |
| OC_{bio} | Ignored |
| OC_{ck} | $\text{POC}_{\text{nf}} - \text{OC}_{\text{bb}}$ |



Table 2. Statistical summary of concentrations, ratios and meteorological parameters at the IAP and PG sites during winter and summer campaigns.

| Compound/ Meteorological parameters | IAP | | | | | | | | PG | | | | | | | |
|--|-----------------|-------|------|-------|-----------------|------|------|-------|-----------------|-------|------|--------|-----------------|------|------|-------|
| | Winter (n = 32) | | | | Summer (n = 34) | | | | Winter (n = 32) | | | | Summer (n = 34) | | | |
| | Mean | Std | Min | Max | Mean | Std | Min | Max | Mean | Std | Min | Max | Mean | Std | Min | Max |
| PM _{2.5} ($\mu\text{g m}^{-3}$) | 97.7 | 75.3 | 8.1 | 328.7 | 30.2 | 14.8 | 12.2 | 78.8 | 99.7 | 77.8 | 13.3 | 294.3 | 27.5 | 12.9 | 11.6 | 70.3 |
| OC($\mu\text{g m}^{-3}$) | 20.5 | 12.2 | 3.9 | 48.8 | 6.4 | 2.3 | 1.8 | 12.7 | 33.2 | 22.0 | 3.8 | 85.0 | 7.7 | 3.4 | 1.8 | 17.9 |
| EC($\mu\text{g m}^{-3}$) | 3.3 | 2.0 | 0.3 | 6.6 | 0.9 | 0.4 | 0.2 | 1.7 | 3.7 | 2.3 | 0.3 | 9.8 | 1.2 | 0.7 | 0.1 | 3.1 |
| OC/EC | 6.9 | 2.4 | 4.1 | 14.9 | 7.6 | 2.2 | 4.6 | 14.8 | 9.0 | 1.9 | 6.2 | 14.6 | 9.0 | 6.7 | 4.4 | 28.3 |
| LG(ng m^{-3}) | 310.7 | 196.0 | 20.4 | 634.7 | 27.9 | 29.6 | 2.9 | 179.6 | 634.3 | 483.2 | 52.1 | 1796.1 | 74.0 | 34.2 | 29.9 | 219.8 |
| MN(ng m^{-3}) | 32.4 | 20.7 | 2.3 | 65.8 | 2.6 | 2.4 | 0.4 | 14.2 | 81.1 | 63.2 | 5.7 | 224.4 | 10.3 | 3.7 | 4.2 | 19.5 |
| GA(ng m^{-3}) | 60.3 | 39.7 | 4.6 | 138.6 | 4.3 | 2.5 | 0.1 | 12.0 | 190.2 | 172.9 | 7.8 | 723.1 | 14.2 | 7.6 | 4.1 | 38.0 |
| K ⁺ ($\mu\text{g m}^{-3}$) | 1.2 | 1.0 | 0.2 | 3.8 | 0.4 | 0.4 | 0.1 | 2.0 | 1.6 | 1.3 | 0.1 | 5.5 | 0.5 | 0.3 | 0.0 | 1.7 |
| WS (m s^{-1}) | 1.4 | 1.2 | 1.5 | 5.6 | 3.6 | 0.8 | 1.9 | 5.6 | 1.4 | 0.8 | 0.5 | 3.4 | 1.1 | 0.6 | 0.4 | 2.5 |
| RH (%) | 41.8 | 15.1 | 18.2 | 80.9 | 43.7 | 16.6 | 18.4 | 85.9 | 51.7 | 13.2 | 32.0 | 78.1 | 50.2 | 14.3 | 30.5 | 84.0 |
| T (°C) | 7.0 | 3.3 | 0.4 | 14.7 | 24.6 | 3.6 | 16.7 | 31.7 | 1.0 | 3.2 | -4.2 | 8.4 | 23.3 | 3.7 | 15.6 | 31.7 |

Std, standard deviation; LG, MN and GA referred to levoglucosan, mannosan and galactosan, respectively; WS, wind speed; RH, relative humidity, T, temperature.



Table 3. Pearson correlations of species at IAP and PG sites.

| IAP winter | PM _{2.5} | OC | EC | K ⁺ | LG | MN | GA |
|-------------------|-------------------|------|-------|----------------|------|------|------|
| PM _{2.5} | 1.00 | | | | | | |
| OC | 0.91 | 1.00 | | | | | |
| EC | 0.86 | 0.92 | 1.00 | | | | |
| K ⁺ | 0.74 | 0.67 | 0.71 | 1.00 | | | |
| LG | 0.56 | 0.60 | 0.74 | 0.51 | 1.00 | | |
| MN | 0.52 | 0.57 | 0.72 | 0.48 | 0.99 | 1.00 | |
| GA | 0.52 | 0.55 | 0.70 | 0.52 | 0.98 | 0.97 | 1.00 |
| PG winter | PM _{2.5} | OC | EC | K ⁺ | LG | MN | GA |
| PM _{2.5} | 1.00 | | | | | | |
| OC | 0.95 | 1.00 | | | | | |
| EC | 0.85 | 0.93 | 1.00 | | | | |
| K ⁺ | 0.88 | 0.78 | 0.70 | 1.00 | | | |
| LG | 0.89 | 0.89 | 0.81 | 0.86 | 1.00 | | |
| MN | 0.85 | 0.85 | 0.82 | 0.84 | 0.94 | 1.00 | |
| GA | 0.88 | 0.85 | 0.74 | 0.84 | 0.95 | 0.94 | 1.00 |
| IAP summer | PM _{2.5} | OC | EC | K ⁺ | LG | MN | GA |
| PM _{2.5} | 1.00 | | | | | | |
| OC | 0.72 | 1.00 | | | | | |
| EC | 0.34 | 0.79 | 1.00 | | | | |
| K ⁺ | 0.65 | 0.64 | 0.36 | 1.00 | | | |
| LG | 0.52 | 0.59 | 0.36 | 0.85 | 1.00 | | |
| MN | 0.47 | 0.55 | 0.37 | 0.80 | 0.97 | 1.00 | |
| GA | 0.41 | 0.59 | 0.54 | 0.59 | 0.79 | 0.85 | 1.00 |
| PG summer | PM _{2.5} | OC | EC | K ⁺ | LG | MN | GA |
| PM _{2.5} | 1.00 | | | | | | |
| OC | 0.60 | 1.00 | | | | | |
| EC | 0.41 | 0.75 | 1.00 | | | | |
| K ⁺ | 0.65 | 0.80 | 0.57 | 1.00 | | | |
| LG | 0.42 | 0.46 | 0.32 | 0.51 | 1.00 | | |
| MN | 0.47 | 0.22 | -0.03 | 0.17 | 0.65 | 1.00 | |
| GA | 0.53 | 0.30 | 0.03 | 0.22 | 0.33 | 0.55 | 1.00 |

LG, MN and GA referred to levoglucosan, mannosan and galactosan, respectively.



Table 4. Comparison of LG concentrations and OC from biomass burning in this study and related literature.

| Site | Site Type | Sampling Time | LG ng m ⁻³ | OC _{bb} contribution | OC/LG used for estimation | Reference |
|-----------|-----------|--------------------------------------|----------------------------------|-------------------------------|---------------------------|-------------------|
| Beijing | Urban | Winter (16 Nov-12 Dec 2016) | 310.7 ± 196.0 | 10.6 ± 1.7% | | This Study |
| Beijing | Urban | Winter in 2013-2014 | 189, 36.1–491 | 12.2%, 3.61–19.5% | 12.29 | Kang et al., 2018 |
| Beijing | Urban | Winter in 2012-2013 | 361, 171–730 | 16.6%, 6.06–35.2% | 12.20–12.50 | Li et al., 2018 |
| Wuhan | Urban | Winter (9 January-6 February 2013) | 950 ± 421 | 21% ± 9% | 7.76 ± 1.47 | Liu et al., 2016b |
| Beijing | Urban | Summer (22 May-22 Jun 2017) | 27.9 ± 29.6 | 6.5 ± 5.2% | | This Study |
| Beijing | Urban | Summer (9 June-8 July 2014) | 56.37 ± 55.48 | 14.8 ± 9.4% | 20.83 | Yan et al., 2019 |
| Beijing | Urban | Summer in 2014 | 12.4, 0.84–26.8 | 2.73%, 0.28–5.60% | 12.29 | Kang et al., 2018 |
| Beijing | Urban | Summer in 2012 | 61.8, 13.9–317 | 8.39%, 2.64–12.5% | 12.20–12.50 | Li et al., 2018 |
| Beijing | Rural | Winter (16 Nov-12 Dec 2016) | 634.3 ± 483.2 | 10.4 ± 1.5% | | This Study |
| Xi'an | Rural | Winter (17-26 January 2014) | 930 ± 320 in PM _{0.133} | 24%, 19–32% | 12.2 | Zhu et al., 2017 |
| Beijing | Rural | Summer (22 May-22 Jun 2017) | 74.0 ± 34.2 | 17.9 ± 3.5% | | This Study |
| Zhengzhou | Suburban | Summer, BB episode in 2-21 June 2015 | 460–1230 | 47.20% | 13.51 | Chen et al., 2018 |
| Zhengzhou | Suburban | Summer, Non-BB in 2-21 June 2015 | 200–290 | 13.90% | 11.9 | Chen et al., 2018 |
| Hebei | Rural | Summer (9 June-8 July 2014) | 205.94 ± 304.35 | 31.3 ± 18.8% | 20.83 | Yan et al., 2019 |



Table 5. Source contribution estimates ($\mu\text{g m}^{-3}$) for OC at IAP and PG in winter and summer.

| Sources | Winter | | | Winter | | | Summer | |
|--|-------------------|---------------------------|-----------------|------------------|--------------------------|-----------------|-----------|-------------|
| | IAP haze (n=5) | IAP non- haze (n=2) | Winter (n=7) | PG haze (n=5) | PG non- haze (n=2) | Winter (n=7) | IAP (n=6) | PG (n=5) |
| EG method results | | | | | | | | |
| Fossil-derived POC (POC_f) | 13.5±3.9 | 3.0±3.5 | 10.5±6.2 | 20.4±2.5 | 5.0±1.3 | 16.0±7.8 | 2.3±0.8 | 3.3±1.9 |
| Biomass burning (OC_{bb}) | 3.4±0.9 | 1.2±0.9 | 2.7±1.3 | 6.1±1.7 | 1.9±0.5 | 4.8±2.4 | 0.6±0.7 | 2.0±0.8 |
| Cooking (OC_{ck}) | 1.3±0.5 | 0.4±0.7 | 1.1±0.7 | 6.8±3.7 | 3.0±0.7 | 5.8±3.6 | 1.1±0.4 | 0.9±0.4 |
| Fossil-derived SOC (SOC_f) | 9.5±3.5 | 3.3±1.3 | 7.7±4.2 | 16.8±10.4 | 4.6±2.6 | 13.3±10.4 | 2.0±0.9 | 2.1±1.5 |
| Non-fossil-derived SOC (SOC_{nf}) | 6.2±2.1 | 1.5±1.0 | 4.8±2.9 | 11.9±9.2 | 1.9±1.0 | 9.1±9.0 | 2.2±2.1 | 3.1±3.1 |
| CMB results | | | | | | | | |
| Gasoline vehicle | 2.8±1.2 | 1.4±0.2 | 2.4±1.2 | 1.6±1.1 | 0.5±0.2 | 1.3±1.0 | 0.4±0.1 | 0.1±0.0 |
| Diesel vehicle | 1.3±2.1 | 0.0±0.0 | 0.9±1.8 | 11.4±3.9 | 1.9±1.5 | 8.7±5.7 | 0.1±0.2 | 0.6±0.3 |
| Industrial CC | 5.5±3.9 | 0.6±0.3 | 4.1±4.0 | 4.9±2.4 | 1.6±0.2 | 4.0±2.5 | 2.1±0.4 | 4.2±2.6 |
| Residential CC | 5.7±4.8 | 2.1±2.3 | 4.6±4.4 | 8.6±4.7 | 3.3±1.4 | 7.1±4.7 | 0.2±0.1 | 0.4±0.2 |
| Vegetative Detritus | 0.1±0.1 | 0.1±0.0 | 0.1±0.1 | 3.3±4.7 | 0.5±0.3 | 2.5±4.1 | 0.2±0.1 | 0.3±0.3 |
| Biomass Burning | 5.5±1.9 | 1.8±1.4 | 4.4±2.5 | 11.6±4.3 | 3.0±0.8 | 9.2±5.5 | 0.6±0.8 | 1.2±0.7 |
| Cooking | 3.6±3.3 | 0.7±0.5 | 2.8±3.1 | 0.2±0.2 | 0.6±0.1 | 0.3±0.3 | 0.6±0.3 | 0.6±0.4 |
| Other OC | 9.4±3.6 | 2.7±2.6 | 7.4±5.7 | 20.2±7.4 | 5.0±2.3 | 15.9±9.6 | 4.0±2.2 | 4.1±2.5 |
| Total OC | 33.8±8.6 | 9.4±7.4 | 26.8±14.2 | 62.0±19.4 | 16.4±6.1 | 48.9±27.3 | 8.3±3.2 | 11.5±4.9 |

CMB results are from Wu et al., 2020 and Xu et al., 2020

CC: coal combustion; Other OC is calculated by subtracting seven primary sources of OC from total measured OC.

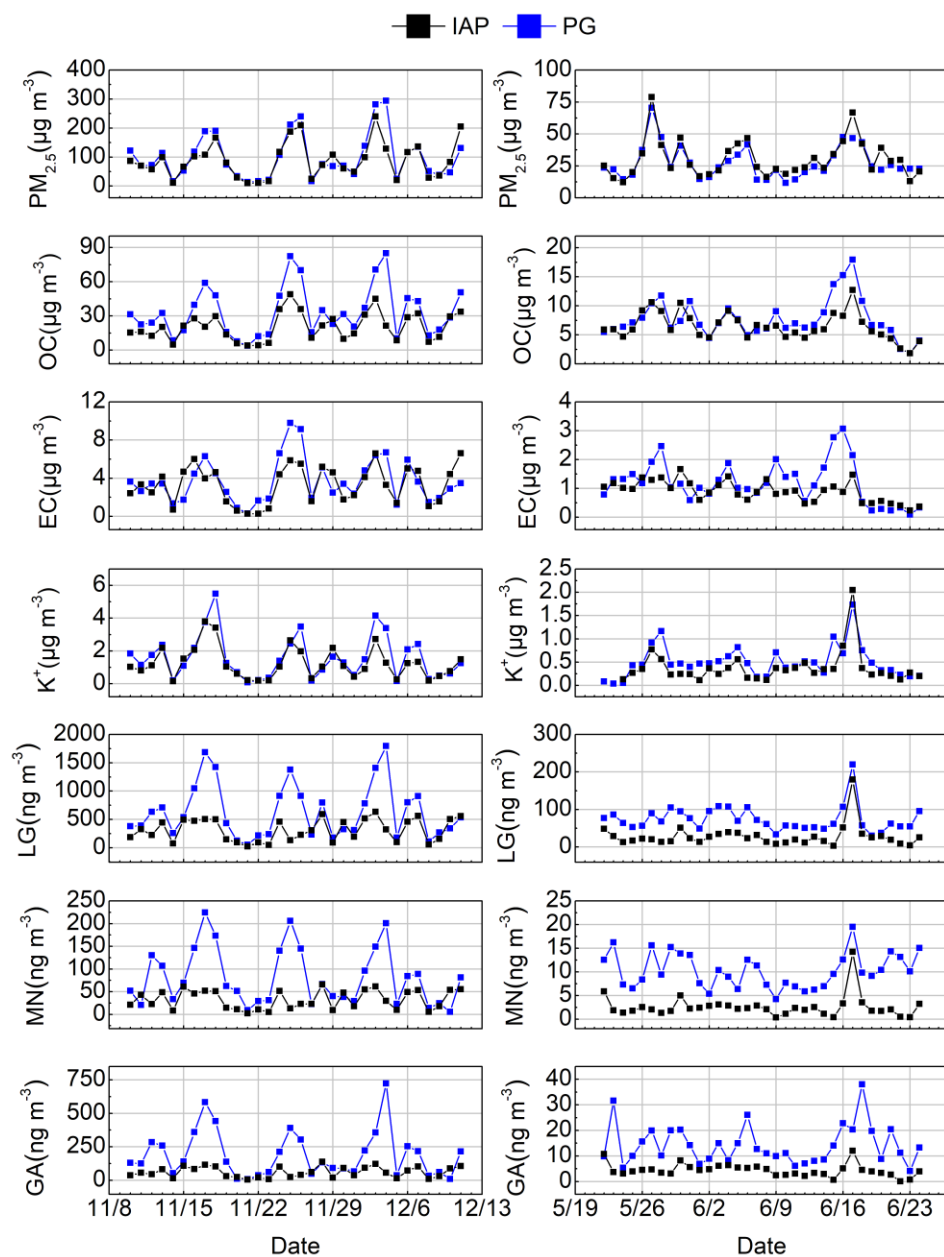


Figure 1. Time series of $\text{PM}_{2.5}$ and its major components at IAP and PG during winter (right) and summer (left).

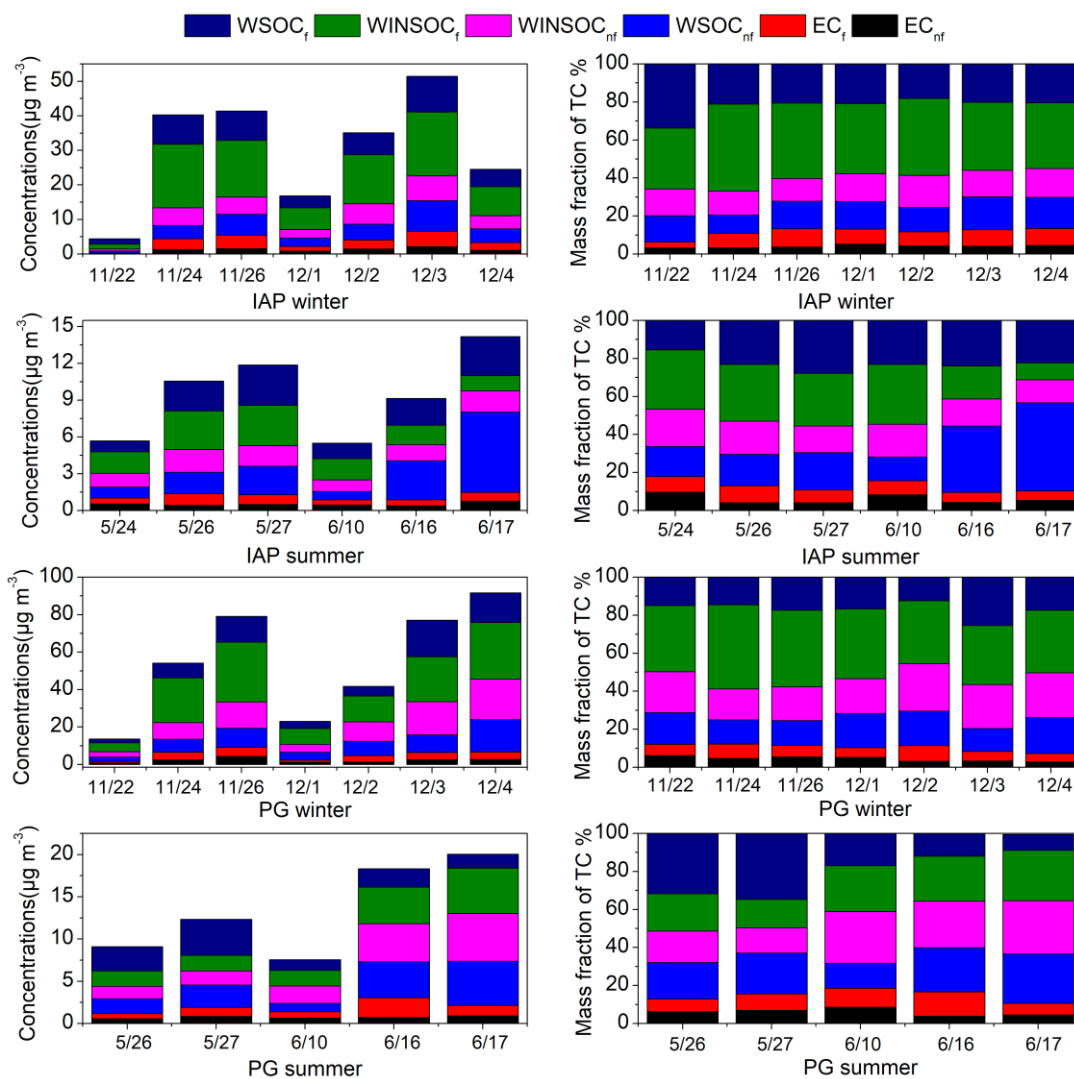


Figure 2. Time series of concentrations of WSOC_f, WSOC_{nf}, WINSOC_f, WINSOC_{nf}, EC_f and EC_{nf} (left) and their relative
 815 contributions to TC (right) at IAP and PG.

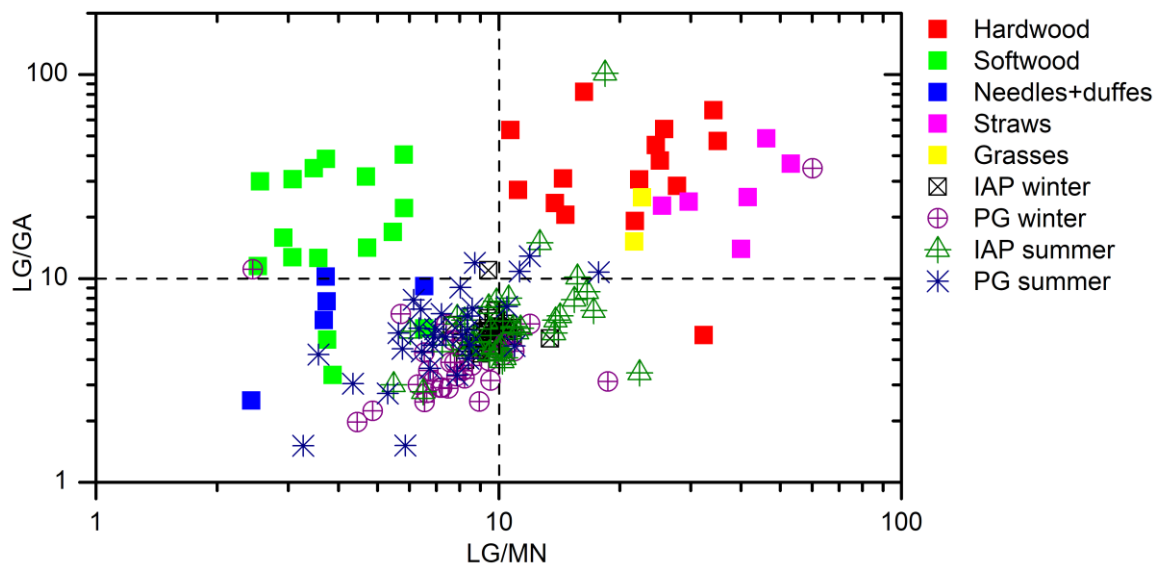


Figure 3. Scatter plot of LG/MN vs. LG/GA from different types of biomass burning emissions (Cheng et al., 2013; Sun et al., 2019b; Sun et al., 2019a), including those measured in PM_{2.5} samples at IAP and PG during winter and summer. The range of LG/MA is 7.66–13.41 and 5.48–22.40 for IAP in winter and summer, 2.45–60.20 and 3.27–17.71 for PG in winter and summer, while the range of LG/GA is 3.98–6.92, 2.78–101.43, 1.97–34.66 and 1.51–13.39, respectively.

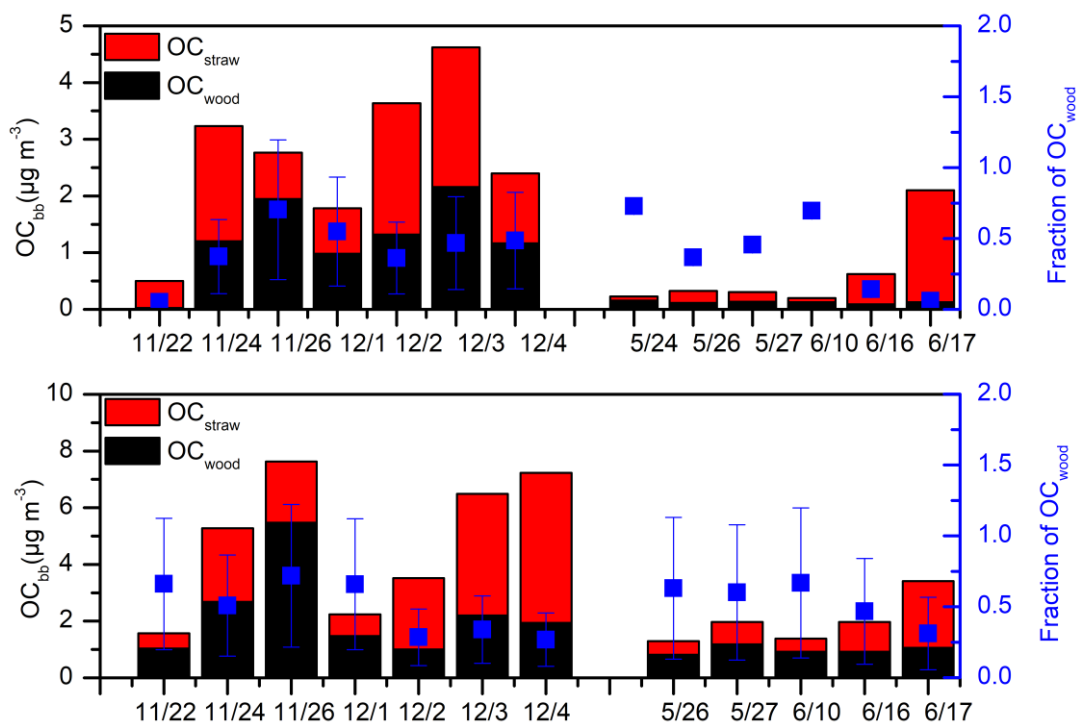


Figure 4. Concentrations of OC from softwood (OC_{wood}) vs. OC from straw (OC_{straw}) at IAP (upper) and PG (lower) and variations of OC_{wood} fractions.

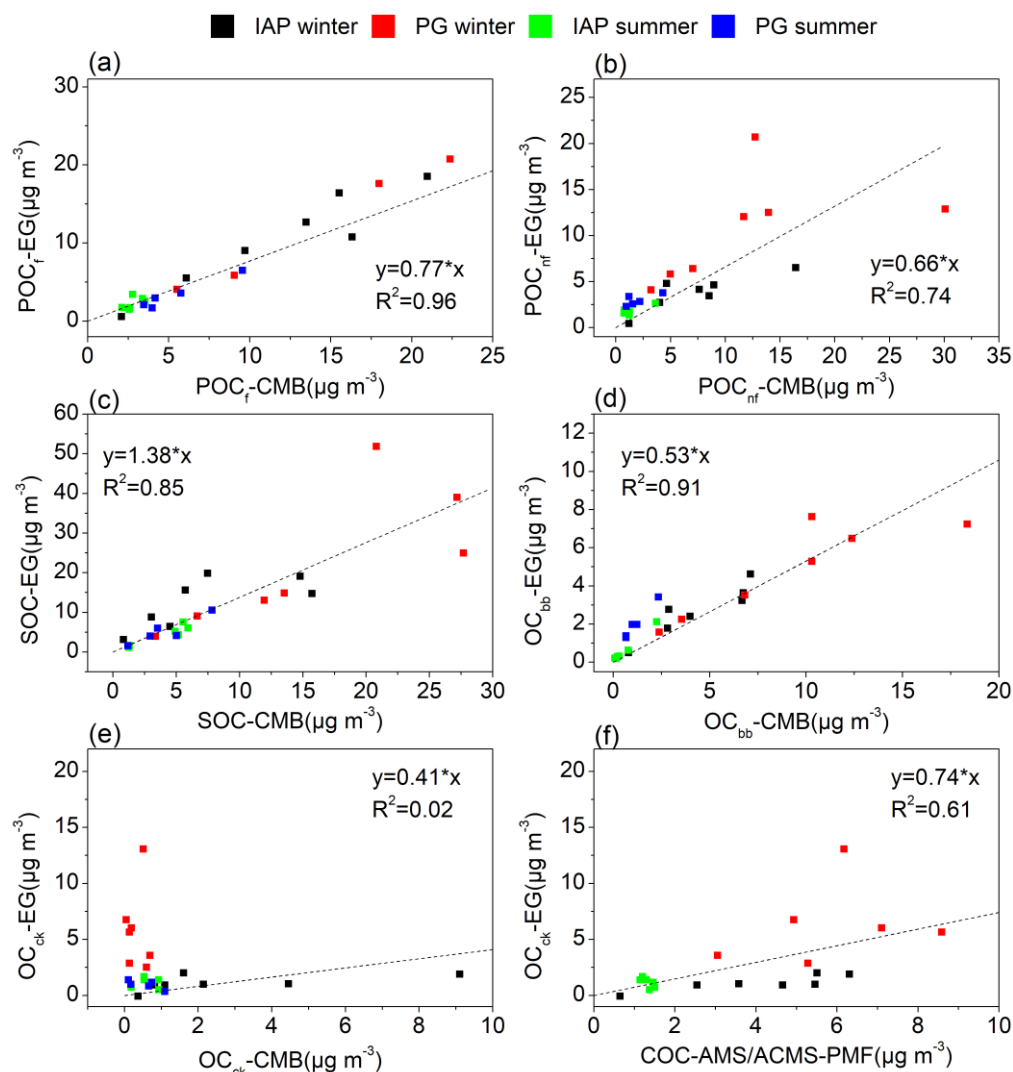


Figure 5. Correlations of OC sources from extended Gelencsér method with those from CMB model. EG denotes extended Gelencsér method, (a): primary OC from fossil sources, (b): primary OC from non-fossil sources, (c): secondary OC, (d): OC from biomass burning, (e): OC from cooking, (f): correlations of OC_{ck} from extended Gelencsér method and AMS/ACMS-PMF model (AMS for IAP and ACMS for PG).

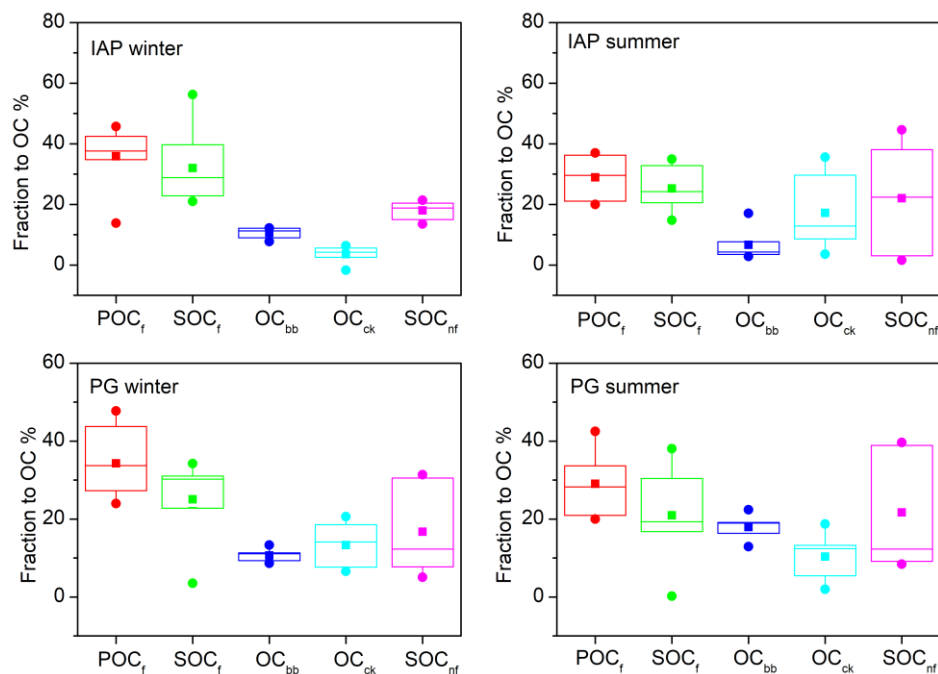


Figure 6. Fractions of each source (i.e., POC_f, SOC_f, OC_{bb}, OC_{ck} and SOC_{nf}) in OC based on the extended Gelencsér method. f: fossil fuel sources, nf: non-fossil sources, bb: biomass burning, ck: cooking. The box denotes the 25th (lower line), 50th (middle line), and 75th (top line) percentiles; the solid squares within the box denote the mean values; the end of the vertical bars represents the 10th (below the box) and 90th (above the box) percentiles; and the solid dots denote maximum and minimum values.

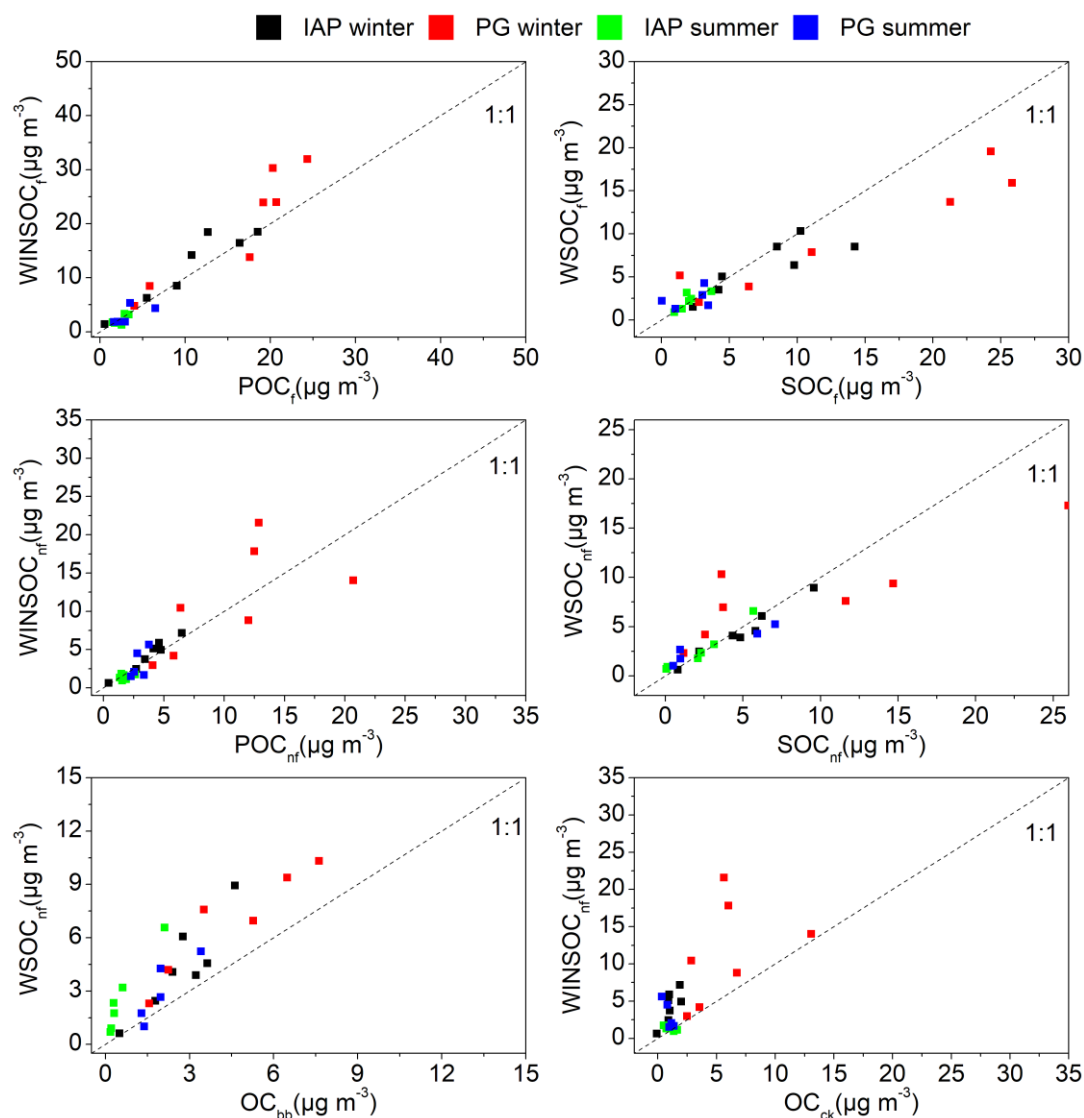


Figure 7. Correlations of WINSOC, WSOC with POC, SOC at IAP and PG sites in winter and summer. The slopes and correlation coefficients are summarized in Table S5.